Monitoring Cerebral Autoregulation in Critically Ill Infants: Exploring the Role of NIRS

Optimizing Mean Arterial Pressure with the Cerebral Oximetry Index (COx)

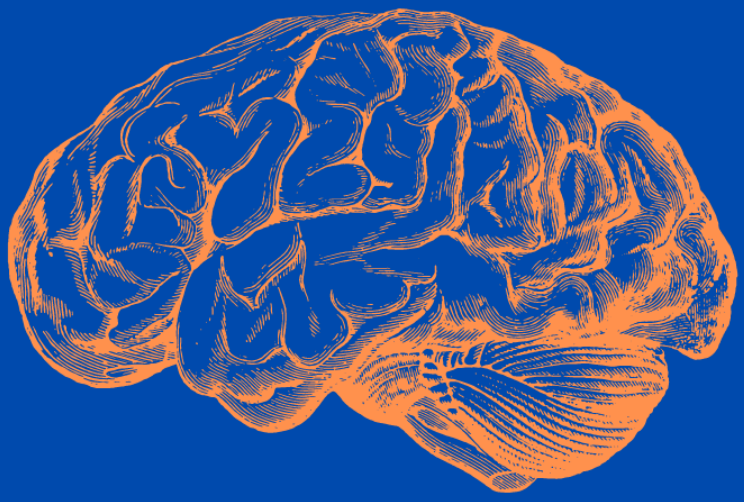

"Providing a Window into the Brain"

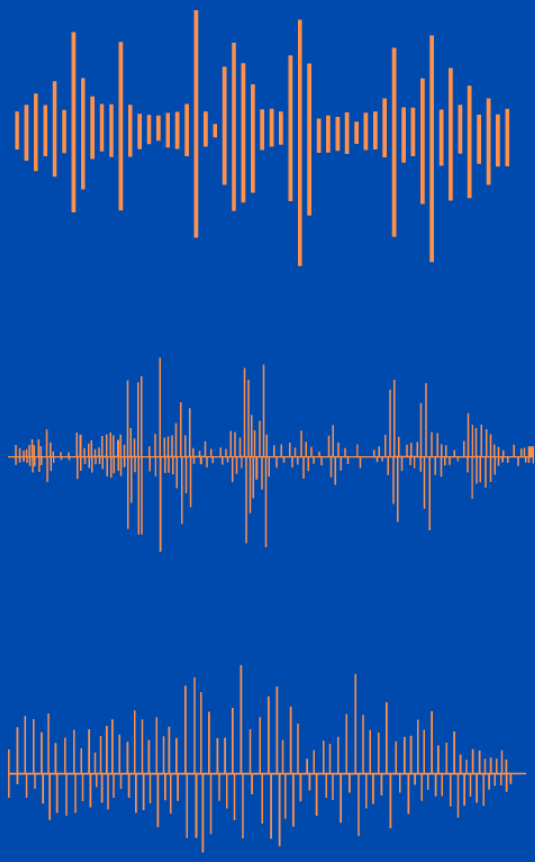

JORIJN VAN DEN BOOM

2024

MSc. Technical Medicine Thesis

Monitoring Cerebral Autoregulation in Critically Ill Infants: Exploring the Role of NIRS

Optimizing Mean Arterial Pressure with the Cerebral Oximetry Index (COx)

by

J.M. van den Boom

Student Name	Student Number
J.M. van den Boom	4664027

Medical Supervisors:	dr. R.C.J. de Jonge, Pediatric Intensivist, PICU, Sophia Children's Hospital
	dr. J.W. Kuiper, Pediatric Intensivist, PICU, Sophia Children's Hospital
Technical Supervisor:	Prof. dr. ir. A.C. Schouten, Professor, Department of Biomechanical Engineering, TU Delft
Daily Supervisors:	drs. E. van Twist, Technical Physician, PICU, Sophia Children's Hospital
	drs. B. van Winden, Technical Physician, PICU, Sophia Children's Hospital
Project Duration:	January, 2024 - December, 2024
Faculty:	Faculty of Mechanical Engineerg (ME), Delft University of Technology

Cover: Design by J.M. van den Boom

Erasmus MC Sophia Children's Hospital

TU Delft

Preface

Het schrijven van deze thesis was een avontuur met pieken, dalen en vooral veel koppen koffie. Gelukkig was ik niet alleen op deze reis, en dat wil ik graag even benadrukken.

Allereerst wil ik mijn begeleiders bedanken voor hun intensieve begeleiding. Bedankt voor de feedback, het geduld en de stroom aan kennis. Dankzij jullie kon ik telkens weer een stap vooruit als ik zelf even helemaal vastzat. Daarnaast ook bedankt voor het openstellen van jullie afdeling in het ziekenhuis waar ik veel heb geleerd en indrukken heb opgedaan. En Eris, dank je wel dat je altijd last minute beschikbaar was voor een goede sparsessie, ongeacht het tijdstip of de deadline die naderde. Jouw inzet, steun en betrokkenheid hebben mij erg geholpen.

Mijn studievrienden van STUK verdienen ook een benaming. Jullie zijn mij allemaal voorgegaan, en nu is het eindelijk mijn beurt om af te studeren (moet niet gekker worden). Het voelt alsof ik als laatste de finishlijn over kruip, maar wat ben ik blij dat we het toch samen een soort van het afsluiten. Onze studietijd was een rollercoaster, van bachelorvrienden naar mastervrienden (en tuurlijk burgervriendinnen), met ontelbare uren in de UB (of waar er dan ook maar plek was op de TU), de ontelbare koppen 'lekkere' koffie en zeker ook de nodige frustratiemomentjes. Maar het was er eentje die ik voor geen goud had willen missen. De momenten dat we samen vastzaten (soms letterlijk om 3mE) en uiteindelijk toch weer een soort van oplossing vonden, dat is STUK. Ik ben wel bij een keertje in de maand een thuiswerkdag in de UB samen trouwens.

Dan mijn familie, jullie hebben me altijd door dik en dun gesteund, ook al begrepen jullie - en ikzelf vaak ook niet - waar ik nou eigenlijk mee bezig was. Jullie vertrouwen en aanmoediging betekenden heel veel voor mij, vooral op die momenten dat ik het zelf even niet meer zag zitten soms. Jullie hebben altijd met me meegeleefd, zonder dat ik ooit hoefde uit te leggen waarom iets belangrijk was of waarom ik me ergens druk over maakte. Bedankt voor het bieden van de stabiliteit en de steun die ik nodig had om deze marathon (overigens de enige die ik ooit zal uitlopen) te voltooien.

En natuurlijk mijn collega's bij Klooster en Doerak, die letterlijk mijn afstudeerjaar draaglijk hebben gemaakt. Bedankt voor de ontspanning, de humor en de energie die ik uit ons werk, barsessies en vroege ochtenden haal. Of het nu ging om een drukke dienst of een rustige avond vol goede gesprekken, jullie waren er altijd om me op te vrolijken en me even te laten ontspannen. Zonder jullie was het studeren echt een stuk zwaarder geweest. Jullie hebben me eraan herinnerd dat het belangrijk is om ook plezier te maken en te genieten , zelfs tijdens een stressvol afstudeerproces (soms iet té misschien). Nu zijn jullie voorlopig nog niet van mij af, want ik moet nog even gaan bedenken wat ik hierna ga doen.

Tot slot, de meiden van Abstract: onze asbstrafstudeerdagen in de UB of bij Civiel op het laatst waren een ware reddingsboei. Jullie sleepten me erdoorheen met motivatie, discipline en de nodige (soms wat lange) koffiepauzes. Van samen in de boot, naar samen elkaar helpen in nood.

Dankzij al deze mensen heb ik de eindstreep gehaald. Op naar de volgende avonturen!

J.M. van den Boom
Delft, November 2024

Abstract

Introduction
In the Pediatric Intensive Care Unit (PICU), maintaining stable cerebral blood flow (CBF) is essential in cirtically ill children, as fluctuations can lead to severe neurological complications. Cerebral autoregulation (CA) ensures stable CBF despite changes in systemic blood pressure. Traditional methods such as intracranial pressure (ICP) monitoring and transcranial Doppler (TCD) provide indirect assessments of CA and are often invasive or limited in continuous monitoring. Near-infrared spectroscopy (NIRS) offers a more non-invasive alternative by continuously measuring cerebral oxygenation. By correlating cerebral regional oxygen saturation ($CrSO_2$) with, though invasive, mean arterial pressure (MAP), the cerebral oximetry index (COx) can be calculated, quantifying the brain's autoregulatory efficiency. This allows clinicians to determine the optimal MAP (MAP_{opt}) per individual, where CA is most effective, which could improve patient outcomes by maintaining stable cerebral perfusion.

Objective
This thesis aims to evaluate COx, derived from ($CrSO_2$) and MAP, to identify the MAP_{opt} in pediatric patients undergoing surgery for congenital diaphragmatic hernia (CDH) or esophageal atresia (EA). Additionally, it examines differences in CA across pre-, intra-, and postoperative phases, providing insights into how surgery affects CA.

Method
Left and right $CrSO_2$ and MAP signals, pre-, intra-, and post-operatively, were retrospectively analyzed to assess CA using the COx. Data preprocessing involved the removal of artifacts, normalization, and signal alignment. COx was calculated as the moving Pearson correlation of $CrSO_2$ with MAP over time using a 5 minute sliding window with a one minute stepsize. Impaired CA was defined as a COx cut-off value ≥ 0.3, defining a correlation between the MAP and $CrSO_2$. The MAP_{opt} was identified as the MAP associated with the lowest COx values, representing the most effective CA. The optimal MAP range was calculated per patient.

Results
CA was interpreted to be most compromised during the intraoperative phase, with elevated COx values in both CDH and EA patient groups. The MAP_{opt} was successfully determined in most cases, showing variability across operative states, with lower values observed intraoperatively. The percentage of time with COx above the cut-off of 0.3 was highest during surgery, especially for EA patients. No remarkable differences were found between the left and right $CrSO_2$ signals.

Conclusion
The study demonstrates the feasibility of using NIRS-derived COx to determine MAP_{opt} in neonates undergoing CDH or EA surgery. These findings highlight the potential for individualized MAP targets to optimize cerebral perfusion, especially during critical surgical interventions.

Contents

Nomenclature

Abbreviations

Abbreviation	Definition
ABP	Arterial Blood Pressure
ANS	Autonomic Nervous System
BFI	Blood Flow Index
CA	Cerebral Autoregulation
CBF	Cerebral Blood Flow
CBFV	Cerebral Blood Flow Velocity
CBV	Cerebral Blood Volume
CDH	Congenital Diaphragmatic Hernia
CO_2	Carbon Dioxide
COx	Cerebral Oximetry Index
CPP	Cerebral Perfusion Pressure
$CrSO_2$	Cerebral Regional Oxygen Saturation
EA	Esophageal Atresia
ECMO	Extracorporeal Membrane Oxygenation
EVD	External Ventricular Drain
FiO_2	Fraction of Inspired Oxygen
Fs	Sampling Frequency
Hb	Deoxygenated Hemoglobin
HbO_2	Oxygenated Hemoglobin
Hz	Hertz
ICP	Intracranial Pressure
In	Intraoperative
IQR	Interquartile Range
L	Left
LLA	Lower Limit of Cerebral Autoregulation
MA	Moving Artifact
MAP	Mean Arterial Pressure
MAP_{opt}	Optimal Mean Arterial Pressure
NaN	Not a Number
NIRS	Near Infrared Spectroscopy
NO	Nitric Oxide
PICU	Pediatric Intensive Care Unit
Po	Postoperative
Pr	Preoperative
R	Right
SD	Standard Deviation
TBI	Traumatic Brain Injury
TCD	Transcranial Doppler
ULA	Upper Limit of Cerebral Autoregulation

1

Introduction

The Pediatric Intensive Care Unit (PICU) is a highly technical environment dedicated to the care of critically ill infants, children, and adolescents facing life-threatening conditions. This specialized unit serves as a hub for multidisciplinary healthcare teams, providing intensive monitoring and advanced therapies tailored to the unique physiological needs of pediatric patients. Among the challenges faced in the PICU, ensuring adequate cerebral perfusion in critically ill children is essential, as fluctuations in cerebral blood flow (CBF) can lead to neurological complications [1]. This particular challenge also rises in the perioperative setting where maintaining stable CBF is as important since surgical procedures and anesthesia induces changes in hemodynamics [2, 3].

Cerebral autoregulation (CA) plays a crucial role in maintaining stable CBF despite variations in systemic blood pressure. Cerebral perfusion pressure (CPP) is defined as the difference between mean arterial pressure (MAP) and intracranial pressure (ICP). The brain maintains adequate perfusion over a wide range of CPP by dynamically adjusting the diameter of its arterioles, either through dilation or constriction. This adaptive mechanism, known as cerebral autoregulation, allows the brain to regulate CBF in response to changes in CPP, thereby preserving oxygen delivery and metabolic function. Figure 1.1 visualizes a schematic representation of the CA mechanism [4]. In the absence of CA, a pressure-passive system emerges where CPP is linearly linked to CBF and thus highly correlated.

Impairment of CA can compromise brain perfusion, increasing the risk of secondary neurological injury following trauma, surgical intervention, or critical illness [5–8]. Traditional monitoring methods, such as invasive ICP measurements or transcranial Doppler (TCD) ultrasound, offer insights but do not provide direct assessments of CA. TCD measures real-time blood flow velocities in the major cerebral arteries, helping to assess hemodynamic changes, while ICP monitoring, mainly used in patients after traumatice brain injury (TBI), evaluates the risk of elevated pressures that could jeopardize cerebral perfusion. However, these methods are either invasive or provide limited information about dynamic CA function [9].

To address this gap, near-infrared spectroscopy (NIRS) has emerged as the technology behind cerebral oximetry index (COx) measurement, providing continuous, non-invasive monitoring of cerebral oxygenation and hemodynamics. NIRS operates by emitting near-infrared light through the scalp to measure changes in the concentration of oxygenated (HbO_2) and deoxygenated hemoglobin (Hb) in brain tissue, which allows for real-time assessment of cerebral regional oxygen saturation ($CrSO_2$) [10]. This capability allows clinicians to dynamically track changes in oxygenation, offering a window into the brain's metabolic state and maybe even help guiding interventions aimed at maintaining optimal cerebral perfusion during critical care in the future.

The COX is a metric that quantifies CA by correlating $CrSO_2$ with systemic blood pressure [8, 9, 11, 12]. COx reflects the degree to which cerebral oxygenation changes in response to fluctuations in MAP and thus the brain's ability to autoregulate its blood flow independent of MAP changes. A low COx value suggests intact autoregulation, where cerebral oxygenation remains stable despite fluctuations in MAP (active system), while a high COx indicates impaired autoregulation, where changes in MAP directly

influence cerebral oxygenation (passive system), placing the brain at risk for hypo- or hyperperfusion [8].

By calculating the moving Pearson correlation between NIRS-derived signals and MAP, it is possible to identify the optimal MAP (MAP_{opt}), which represents the pressure range where CA is most effective. Identifying this optimal range allows clinicians to target MAP_{opt} during surgery or critical care, with the aim of reducing the risk of cerebral hypo- or hyperperfusion and thereby preventing secondary neurological injury [8].

This thesis aims to investigate the feasibility and effectiveness of using COx, calculated from the correlation between left/right $CrSO_2$ and MAP, to assess CA in pediatric patients undergoing surgical procedures for congenital diaphragmatic hernia (CDH) or esophageal atresia (EA). The choice to focus on CDH and EA patients was driven by several factors: 1) both patient groups typically undergo surgery, providing an opportunity to assess CA in the perioperative setting; 2) they represent a relatively homogeneous population, which helps minimize variability; 3) a prospective dataset with high-frequency data on $CrSO_2$ and MAP is available as a result of an earlier study performed on these patients, *the NeMo study*; 4) .

The primary goal of this research is to evaluate the feasibility of using the COx, derived from $CrSO_2$ and MAP, to enhance cerebral perfusion in pediatric patients undergoing surgical procedures for CDH or EA. To achieve this, the study aims to fulfill two subgoals. The first subgoal is to determine the MAP_{opt} for each patient by calculating the COx in the pre-, intra-, and postoperative phase, and thus identifying the MAP that may enhance CA in critically ill neonates. The second subgoal is to assess potential differences in CA between the three operative states, thereby offering insights into the effects of surgical interventions on CA. This enhances the understanding of the dynamic relationship between cerebral oxygenation and blood pressure in the perioperative setting. Identifying MAP_{opt} may help guide clinical interventions, ensuring that pediatric patients undergoing surgery for CDH or EA maintain stable cerebral perfusion during surgical procedures.

It is hypothesized that the COx, derived from the correlation between $CrSO_2$ and MAP, will identify the MAP_{opt} for optimal CA. Additionally, it is expected that COx will differ between the three operative states, with a notable difference during the intraoperative phase compared to the pre- and postoperative phases.

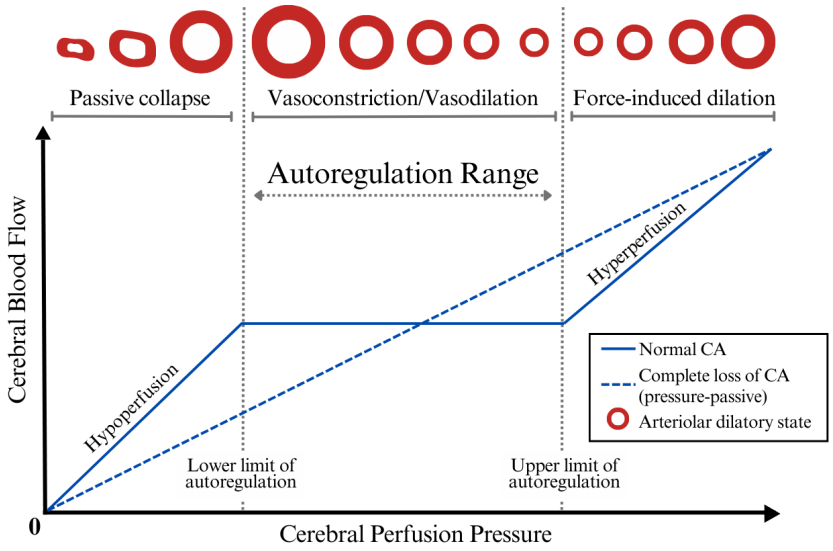

Figure 1.1: A schematic representation of the mechanism of cerebral autoregulation (CA) with the corresponding arteriolar dilatory state. The continuous line displays the normal CA curve; when the cerebral perfusion pressure (CPP) has a value between the lower and upper limit of autoregulation, the cerebral blood flow (CBF) is maintained stable by the CA by changing the arteriolar dilatory state. Below the lower and above the upper limit of autoregulation, the relation between CBF and CPP is pressure passive which can lead to secondary injury. The dotted line shows a pressure passive relation between CPP and CBF and thus a complete loss of CA. [4]

2

Method

2.1. Study Population

The CDH dataset was collected in a multicenter, observational, prospective study on perioperative neuromonitoring in neonates with CDH and EA undergoing surgery. All EA and CDH patients, included in this current study, underwent surgery at the Sophia Children's Hospital in Rotterdam. The data set available was collected as part of *The NeMo CDH/EA Study*: Neuromonitoring during surgical treatment of congenital diaphragmatic herniaor esophageal atresia, NL6972, URL: https://www.trialregister.nl/trial/6972.

Eligible neonates required surgical repair within the first 28 days of life between July 2018 and July 2020, regardless of surgery type (minimal access or open) or ECMO therapy before surgery. Exclusion criteria included major cardiac or chromosomal anomalies, syndromes associated with altered cerebral perfusion, and in addition for the EA group being on ECMO at surgery start.

The sophia Children's Hospital followed standardized perioperative management protocols, with the anesthesia approach reflecting local practices [13]. The dataset used for analysis included data gathered under these conditions, providing an opportunity to study CA in a specific and clinically important patient group [14].

Neonates, included in the *The NeMo CDH/EA Study*, were eligible for inclusion in this data analysis. All patients with continuous $CrSO_2$ and MAP data of at least one operative state (pre-, peri- or postoperative monitoring) were eligible for inclusion in the data analysis of this thesis. Medication administration in either operative state were incorporated in a later stage, as some medicines may have effect on the signals ($CrSO_2$ and/or MAP) [15–18].

2.2. Data Acquisition

The non-invasive neuromonitoring data was collected from the Erasmus MC server where the monitoring data is stored (Draeger, Lübeck, Germany) and the electronic health record employed in Erasmus MC (HiX, Chipsoft, Amsterdam, the Netherlands). The patient characteristics and medication administrations were gathered from the database compiled by *The NeMo CDH/EA Study* and restructured by Hendrikx et al. [14].

The $CrSO_2$ signals were continuously acquired using NIRS before, throughout and/or after the surgical procedures. NIRS probes (NIRS, INVOS 5100C, INVOS®System, Somanetics) were placed bilaterally on the patient's forehead to monitor the $CrSO_2$ in both hemispheres. Simultaneously, MAP was measured using standard invasive arterial blood pressure monitoring, providing real-time data on the systemic hemodynamics. The $CrSO_2$ and MAP signals were recorded at a sampling frequency (Fs) of 1 Hertz (Hz). A schematic representation of the data can be seen in Figure 2.1.

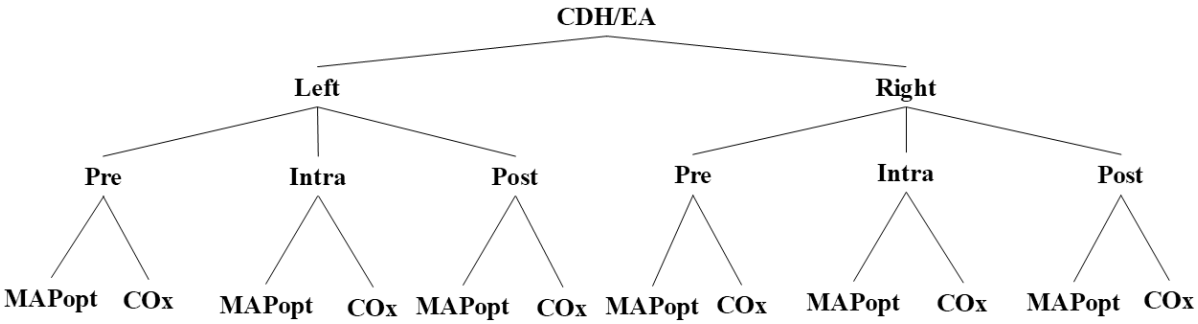

Figure 2.1: Schematic overview of the data distribution for both patientgroups leading to the parameters derived with the algorithm developed in this study. (CDH = congenital diaphragmatic hernia, EA = esophagael atresia, COx = cerebral oximetry index, MAP_{opt} = optimal mean arterial pressure)

2.3. Data Processing

The processing and analyses were performed using *Excel* (Version 2410 Build 16.0.18129.20100, Microsoft, Microsoft Corporation) and *MATLAB* (R2024a, The Mathworks, Natick, US) with the additional toolboxes of *curve_fitting_toolbox* and *signal_toolbox*.

Normalization

To account for baseline differences between left and right and focus on relative trends rather than absolute values, the $CrSO_2$ signals were normalized using z-score normalization. This was done in the first steps of this research to determine whether to combine the left and right $CrSO_2$ signals or to use them separately for the further analysis. The decision was based on a visual inspection of the data, carried out in consultation with the supervisory team.

Given that the focus was on identifying relative changes in the signals rather than absolute values, z-score normalization was chosen over other normalization methods to highlight changes relative to its own mean and standard deviation (SD). This decision was also made because z-score normalization provides a standardized scale that preserves the structure of the data without compressing the range, making it more suitable for trend analysis. For each $CrSO_2$ signal (left and right), the mean was subtracted, and the result was divided by the SD, transforming the signals to have a mean of 0 and a SD of 1. This step ensured that variations in the signals were comparable across time and between patients.

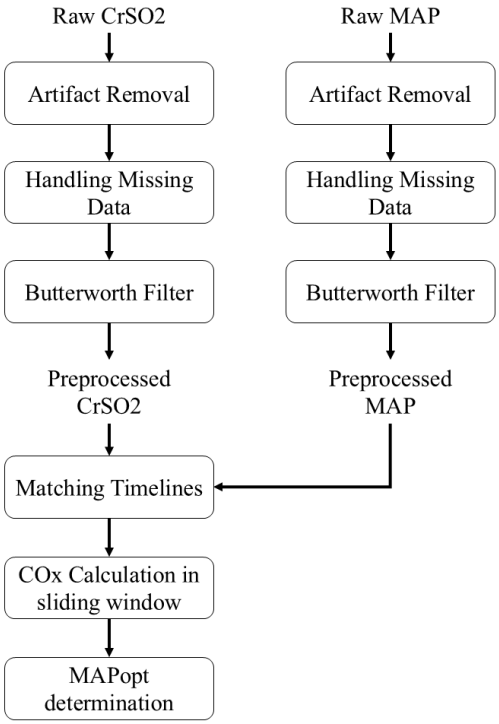

Figure 2.2: Schematic overview of the data processing pipeline used to compute the COx calculations and the MAP_{opt}. ($CrSO_2$ = Cerebral regionl Oxygen Saturation, COx = cerebral oximetry index, $MAP_{(opt)}$ = (optimal) mean arterial pressure)

2.3.1. Preprocessing

To ensure reliable signals for CA analysis, several preprocessing steps were applied to the $CrSO_2$ and MAP data. Figure 2.2 presents a schematic overview of the signal processing pipeline; the different blocks are discussed in the following sections. A detailed pipeline of the preprocessing can be found in appendix A, Fig. A.1.

Artifact Removal

To eliminate noise and artifacts, outlier removal was performed on both $CrSO_2$ and MAP signals [14]. For $CrSO_2$ all data points were restricted to the physically plausible range of 20-100% cerebral oxygen saturation. Any values outside this range were considered physiologically irrelevant and removed. For the left and right $CrSO_2$, motion artifacts (MA) were identified and discarded. MA were defined as

moving SD > 3 in 10 second windows, based on the assumption that MA most often result in signal changes more quickly than expected [19].

Similar to the $CrSO_2$, moving artifacts were discarded from the MAP data. The MAP values were restricted to the physical range of 5-100 mmHg, ensuring that any extreme values outside this range were excluded from the analysis. Note that with discarding the samples they are set to NaN.

Rejected Data
Rejected data points, which were represented as NaNs in the $CrSO_2$ and MAP signals due to the artifact removal step, were calculated as percentage of the raw signal and stored. The following step, filtering, could not handle any NaNs, therefore handling the NaNs in the signals was crucial. The identified NaN segments were handled using linear interpolation or removal. This approach allowed for the estimation of missing values by creating a straight-line interpolation between the known data points. Short gaps (less than 5 minute) were interpolated, while longer gaps were removed. This method was chosen to maintain the continuous trend of the data (which is clinically as important as the exact values [20–22]) without introducing abrupt changes that could distort subsequent analyses.

If a NaN segment was deleted in the MAP signal, the segment with the same indices was also deleted in the $CrSO_2$ signal, and vice versa. This was done to ensure the alignment of the timestamps of the signals for the calculation of the correlation between the signals (i.e., the COx). The MAP signal was first evaluated for NaN segments to be deleted, since both left and right $CrSO_2$ signals needed to be correlated with the MAP (see Figure A.1 in App. A for a detailed overview of the processing pipeline).

The percentages of the deleted and interpolated sample points of the total sample points of each trimmed signal were calculated. After the NaN detection, NaNs in the beginning and end of the signal were located and the signals were trimmed accordingly. These deleted NaNs were not considered in the calculation of these parameters since they would not have an effect on the results. However, NaNs in the middle of signal might have an effect which is why the percentages of these NaNs being deleted or interpolated were tracked and stored.

Filtering
Following the artifact removal, a low-pass Butterworth filter was applied to the $CrSO_2$ and MAP signals for additional noise reduction. The link between slow vasogenic changes in $CrSO_2$ and ABP (slow waves in the 0.05–0.003 Hz range) is reflected in the COx, therefore the Butterworth filter had a cutoff frequency of 0.05 Hz [23]. The Butterworth filter was chosen for its flat frequency response in the passband, which reduces high-frequency noise without introducing phase distortions. A zero-phase filtering approach was implemented by applying the filter forward and then backward in time with the MATLAB function *filtfilt*. This bidirectional filtering ensures that there is no phase shift introduced into the filtered signals, which maintains the alignment of the $CrSO_2$ and MAP signals for subsequent correlation analysis.

Matching Timelines
Before conducting the moving correlation analysis, the $CrSO_2$ and MAP signals were synchronized in time. This step was necessary to ensure that the moving window correlation calculations compared signals at corresponding time points.

2.3.2. Cerebral Oximetry Index (COx)
To assess CA, the COx was calculated by correlating the MAP with left or right $CrSO_2$. The COx was computed by applying a moving Pearson correlation between the MAP and $CrSO_2$ over a sliding window. The Pearson correlation coefficient is a statistical measure that quantifies the strength and direction of a linear relationship between two variables, with values ranging from -1 to 1. In the context of CA, the relationship between MAP and $CrSO_2$, as measured by NIRS from the left and right sides of the brain, is of most interest. By calculating the COx over time, it is possible to assess how $CrSO_2$ responds to fluctuations in MAP.

A Pearson's correlation of -1 indicates a perfect negative linear relationship, while a value of 1 indicates a perfect positive linear relationship. A value of 0 implies no linear relationship between the variables. In the context of CA, a negatively or close to 0 COx value indicates intact CA, meaning that $CrSO_2$ and MAP are either negatively or not correlated, which suggests effective CA. COx values approaching 1

suggest impaired CA, where $CrSO_2$ tracks changes in MAP, indicating reduced CA effectiveness. The COx cut-off value for impaired CA was set at 0.3, conform previous research by Kirschen et al. [8].

For this analysis, a 5-minute window (i.e., 300 samples) was used to calculate the correlation between MAP and the left and right $CrSO_2$. To ensure sufficient temporal resolution while capturing the trend, the window was shifted by 1 minute, resulting in an 80% overlap between consecutive windows. This overlap improves the smoothness of the COx signal and reduces the impact of short-term noise or fluctuations. This extends the traditional Pearson correlation by applying it over the sliding time window across the signals. Thus, this method works as follows:

1. A window of fixed length (5 minutes) is defined, and the Pearson correlation is computed between the MAP and $CrSO_2$ signals for the data points within that window.
2. The window is then shifted by a smaller step (1 minute), and the Pearson correlation is recalculated for the new window.
3. This process is repeated across the entire time series, resulting in a series of correlation coefficients that reflect the dynamic relationship between MAP and $CrSO_2$ over time.

The Pearson correlation coefficient (or thus the COx) was calculated for each window using the following equation:

$$\text{COx} = \frac{\sum(x_i - \bar{x})(y_i - \bar{y})}{\sqrt{\sum(x_i - \bar{x})^2 \sum(y_i - \bar{y})^2}} \tag{2.1}$$

where x_i represents the MAP values within the window, y_i represents the $CrSO_2$ values, and $\bar{x}$ and $\bar{y}$ are their respective means. This calculation was performed for both the left and right $CrSO_2$ signals, providing two separate COx trends for each patient. By sliding the window across the time series, a continuous, time-varying estimate was obtained of the COx over the course of the procedure.

With the 5 minute window size and 1 minute step size one COx value for each minute of data is obtained, resulting in a frequency of approximately 0.0167 Hz for the COx trend. This relatively low frequency reflects the smoothing effect of the moving window and the step size, which allows for the assessment of longer-term trends in CA rather than capturing high-frequency fluctuations. The dynamic COx values were further analyzed to assess the CA during the pre-, intra-, and post-operative phases.

2.3.3. Optimal Mean Arterial Pressure (MAP_{opt})

To assess CA and determine the MAP_{opt} in every patient, the dynamic relationship between MAP and COx was analyzed. The MAP_{opt} represents the level of MAP at which CA is most effective, identified as the MAP associated with the lowest COx value. The optimal MAP range was defined as the MAP values where the optimal COx values are expected based on the patient's individual MAP-COx curve. This is the range between the lower limit (LLA) and the upper limit of CA (ULA), where the MAP-COx curve intersects the COx cut-off value. A schematic overview of the MAP-COx curve is visualized in Figure 2.3. Linking this figure to figure 1.1 in the introduction, the MAP_{opt} lies within the autoregulation range (between the LLA and ULA).

After the COx calculation, the resulting COx values were binned according to corresponding MAP ranges (e.g., 5 mmHg intervals). In order to avoid ceiling effects, the Fisher transform was applied to the binned COx values [8, 24]. For each bin, the mean COx was calculated, and a second order polynomial was fitted on the mean COx values per bin. The MAP_{opt} was defined as the nadir of the fitted curve; the MAP that

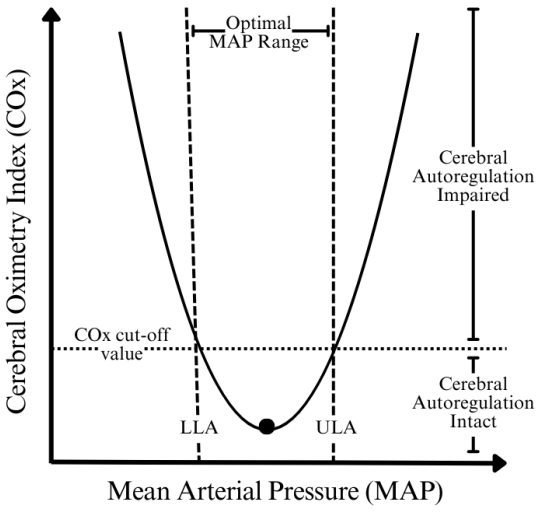

Figure 2.3: Schematic visualization of the MAP-COx curve with the lower and upper limit of cerebral autoregulation (LLA, ULA). With the dot being the optimal MAP (MAP_{opt}).

exhibited the lowest mean COx for each patient. This approach helps identify the MAP range at which the patient's CA is optimally maintained, providing a target for blood pressure management. The second order polynomial could only be fitted if the number of bins was ≥ 3 per operative state and $CrSO_2$ side, since it forms a parabolic curve and therefore needs at least 3 points.

2.4. Analysis

Overview of Data Availability

Analysis of data completeness was carried out to assess the availability of $CrSO_2$ and MAP signal for each patient in both the CDH and EA patient groups. The completeness of $CrSO_2$ and MAP data after preprocessing was evaluated for three operative states; preoperative (Pr), intraoperative (In) and postoperative (Po). Data was classified as either available (1) or not available (0) for each state, patient and $CrSO_2$ side (left or right). This assessment helped provide insights into how representative the dataset is and identify potential biases introduced due to missing data.

Derived Parameters

For each patient, COx was calculated for both the left and right cerebral hemispheres when available. The overall COx trends were analyzed per operative state and patient group and the following parameters were derived:

- Mean COx, indicating the overall level of CA for each state.
- Percentage of time with COx > 0.3, used as an indicator of impaired CA.
- Mean MAP_{opt}, the optimal MAP at which CA was most effective.
- COx at MAP_{opt}, evaluating the effectiveness of CA at the MAP_{opt}.

The distributions of the parameters across each operative state (preoperative, intraoperative, and postoperative) for both the CDH and EA patient groups were visualized using boxplots. Each operative state was represented by two boxplots: one for the CDH group and one for the EA group. The boxplots provide a summary of the distribution, including the median, interquartile range (IQR), and spread of the parameters, thereby offering an overview of CA across the operative windows.

3

Results

3.1. Study Population and Characteristics

For the CDH group 45 patients were included of a total of 48 and for the EA group 27 were included from a total of 35 patients as depicted in Figure 3.1.

Patient and surgery characteristics are shown in Table 3.1. The majority of patients in the CDH group were male (60.0%), while a smaller proportion of the EA group were male (40.74%). The median gestational age was slightly higher for the CDH group (38+1 weeks [37+1 - 38+5]) compared to the EA group (37+2 weeks [35+2 - 39+6]). Patients with CDH underwent surgery at a median age of 4 days [3 - 6], whereas EA patients had surgery earlier, at a median age of 2 days [1 - 3]. Open surgery was more common in the CDH group (66.67%), while thoracoscopic surgery was equally common in both groups (48.15% for EA and 33.33% for CDH). Conversion from thoracoscopic to open surgery was required in 20.0% of CDH cases and 14.81% of EA cases.

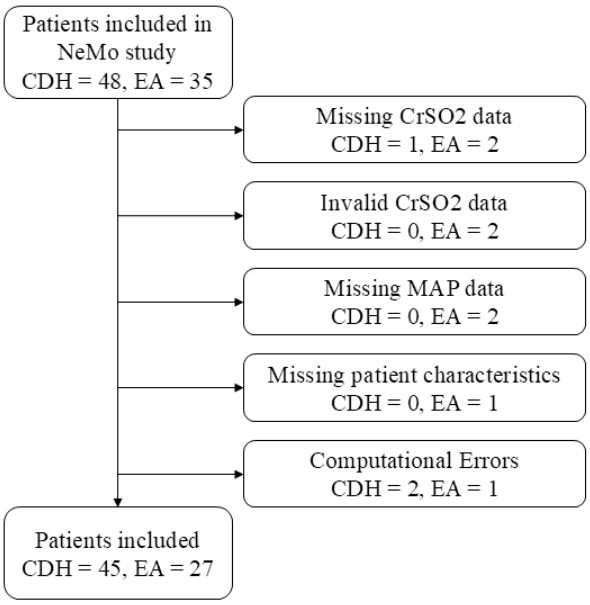

Figure 3.1: Flow chart visualizing the patient inclusions. (CDH = congenital diaphragmatic hernia, EA = esophagael atresia, MAP = mean arterial pressure, $CrSO_2$ = cerebral regional oxygen saturation)

Table 3.1: *Patient Characteristics*

	CDH	EA
Patients	45 (100%)	27 (100%)
Male	27 (60.0%)	11 (40.74%)
Birth weight (grams)	3000 [2688 - 3300]	2900 [2015 - 3183]
Gestational Age	38+1 [37+1 - 38+5]	37+2 [35+2 - 39+6]
Age at surgery (days)	4 [3 - 6]	2 [1 - 3]
Open Surgery	30 (66.67%)	13 (48.15%)
Thoracoscopy Surgery	15 (33.33%)	13 (48.15%)
Conversion Surgery	9 (20.0%)	4 (14.81%)

Note. Values are represented as median [IQR] or N (%). (CDH = Congenital Diaphragmatic Hernia, EA = Esophageal Atresia)

3.2. Preprocessing

Overview Rejected Data

Before preprocessing the signals the NaNs were determined for both MAP and $CrSO_2$, these include all NaNs throughout the whole signal. The highest median percentage of NaNs for the MAP signals is seen in the intraoperative state for both CDH and EA, while no trend was observed in the $CrSO_2$ signals (Table 3.2). The mean (SD) percentage of NaNs in the raw $CrSO_2$ was 10.44% (17.64) for CDH and 8.95% (16.63) for EA, while MAP signals showed 5.04% (8.24) and 16.72% (19.33), respectively. Appendix A.1 Shows an overview of the NaN percentages per group and operative state.

Table 3.2: *Percentage of NaNs in the mean arterial pressure (MAP) and $CrSO_2$ signals over all states, patients and sides (for $CrSO_2$) per group. Values are represented as mean (standard deviation).*

	CDH	EA
NaN % $CrSO_2$	10.44% (17.64)	8.95% (16.63)
NaN % MAP	5.04% (8.24)	16.72% (19.33)

Note. CDH = Congenital Diaphragmatic Hernia, EA = Esophageal Atresia

Figure 3.2 illustrates the artifact removal and filtering applied to the MAP signal, with smoothing observed. Figure A.2 visualizes the preprocessing steps for $CrSO_2$ signals. The mean (SD) percentage of interpolated data was 0.49% (0.95) for $CrSO_2$ and 1.15% (1.01) for MAP in the CDH group, and 0.42% (0.60) for $CrSO_2$ and 1.62% (1.95) for MAP in the EA group. $CrSO_2$ signals showed a higher percentage of deleted points than MAP (Table 3.3). The percentage of the signal that are interpolated varies between groups and states (see the Tables in App. A). Figure 3.3 shows the final preprocessed signals with interpolated or deleted visualized, the resulting COx curve is plotted in the last row of the figure with the cutoff value.

Table 3.3: *Percentage of deleted and interpolated samples in the mean arterial pressure (MAP) and $CrSO_2$ signals over all states, patients and sides (for $CrSO_2$) per group. Values are represented as mean (standard deviation).*

	CDH	EA
Deleted % $CrSO_2$	3.39% (8.45)	3.54% (9.09)
Deleted % MAP	1.28% (3.68)	2.56% (5.34)
Interpolated % $CrSO_2$	0.49% (0.95)	0.42% (0.60)
Interpolated % MAP	1.15% (1.01)	1.62% (1.95)

Note. CDH = Congenital Diaphragmatic Hernia, EA = Esophageal Atresia

Data Availability after Preprocessing

The completeness of the $CrSO_2$ signals is evaluated for the three operative states and the left and right side after preprocessing. Figure 3.4A and 3.4B give a schematic representation of the data distribution for each patient group (see the tables in Appendix A.1 for exact numbers). For both the CDH and EA groups, not all patients have complete data for all three states, see Table A.5. In the CDH group, 82.22% of the patients have data for all states, whereas in the EA group, 22.22% of the patients have data for all states. Some patients have data available for only one (CDH = 0.00%, EA = 14.15%) or two (CDH = 11.11%, EA = 48.15%) states. The availability of the left and right $CrSO_2$ also varies (Table A.5). In the CDH group, 4.44% of patients have only one side (the left side) of the $CrSO_2$ data available, while in the EA group, this percentage is 18.52% (14.81% have only the left side and 3.70% had only the right side).

When assessing the availability of data across different operative states, certain trends emerge which can be seen in Table A.6 in Appendix A.1. Preoperative data for the EA consists of only 33.33% for the left side and 22.22% for the right side. The CDH group has respectively 91.11% and 86.67% availability for the left and right $CrSO_2$ signal preoperatively. Intraoperative and postoperative data have higher availability across both groups.

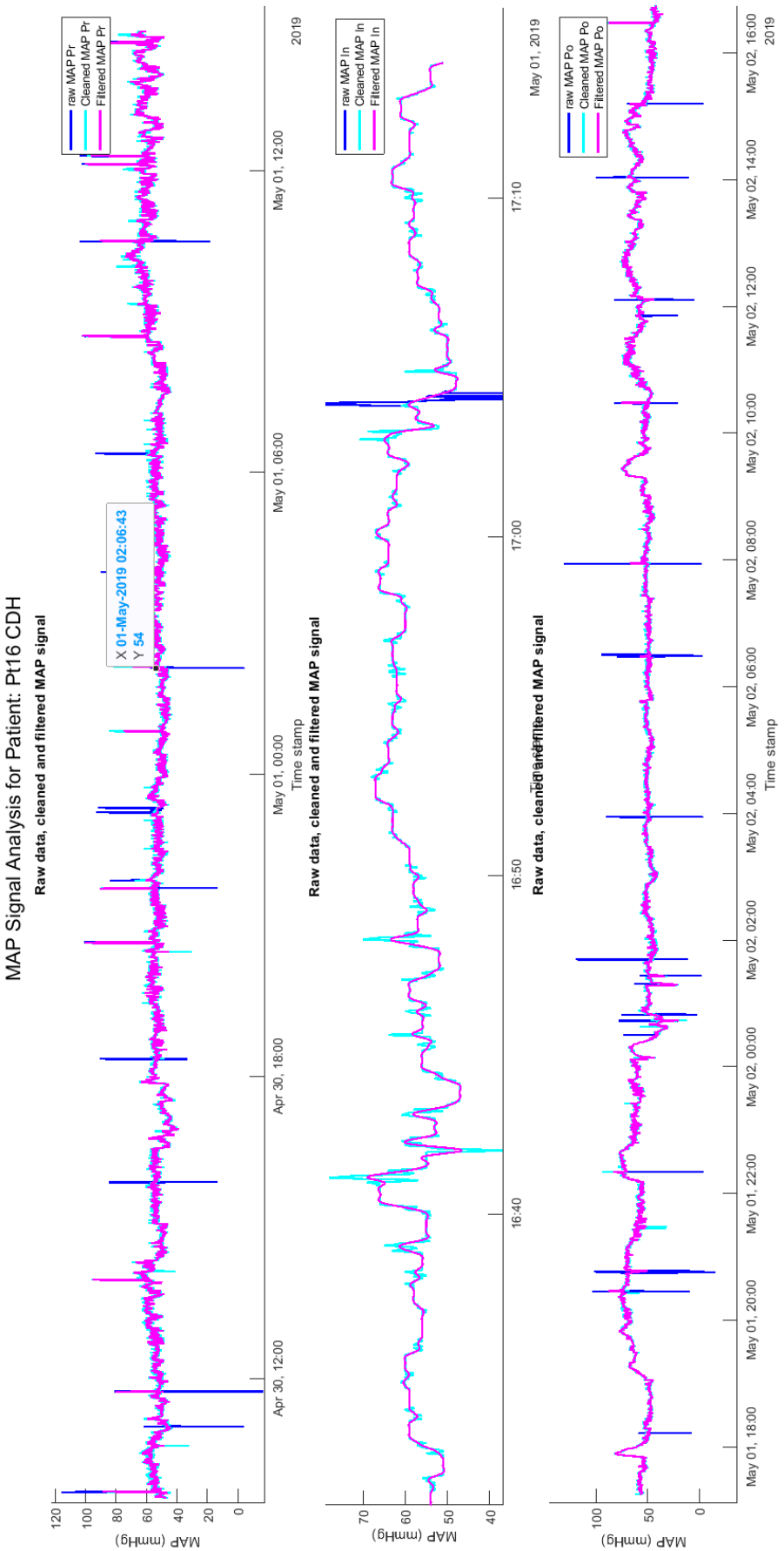

Figure 3.2: Preprocessing of the mean arterial pressure (MAP) signal for each operative window of a random patient. With dark blue being the raw signal, the light blue the cleaned signal (after artifact removal) and the pink the filtered signal used for the further analysis. *Note:* The intraoperative MAP signal is zoomed in.

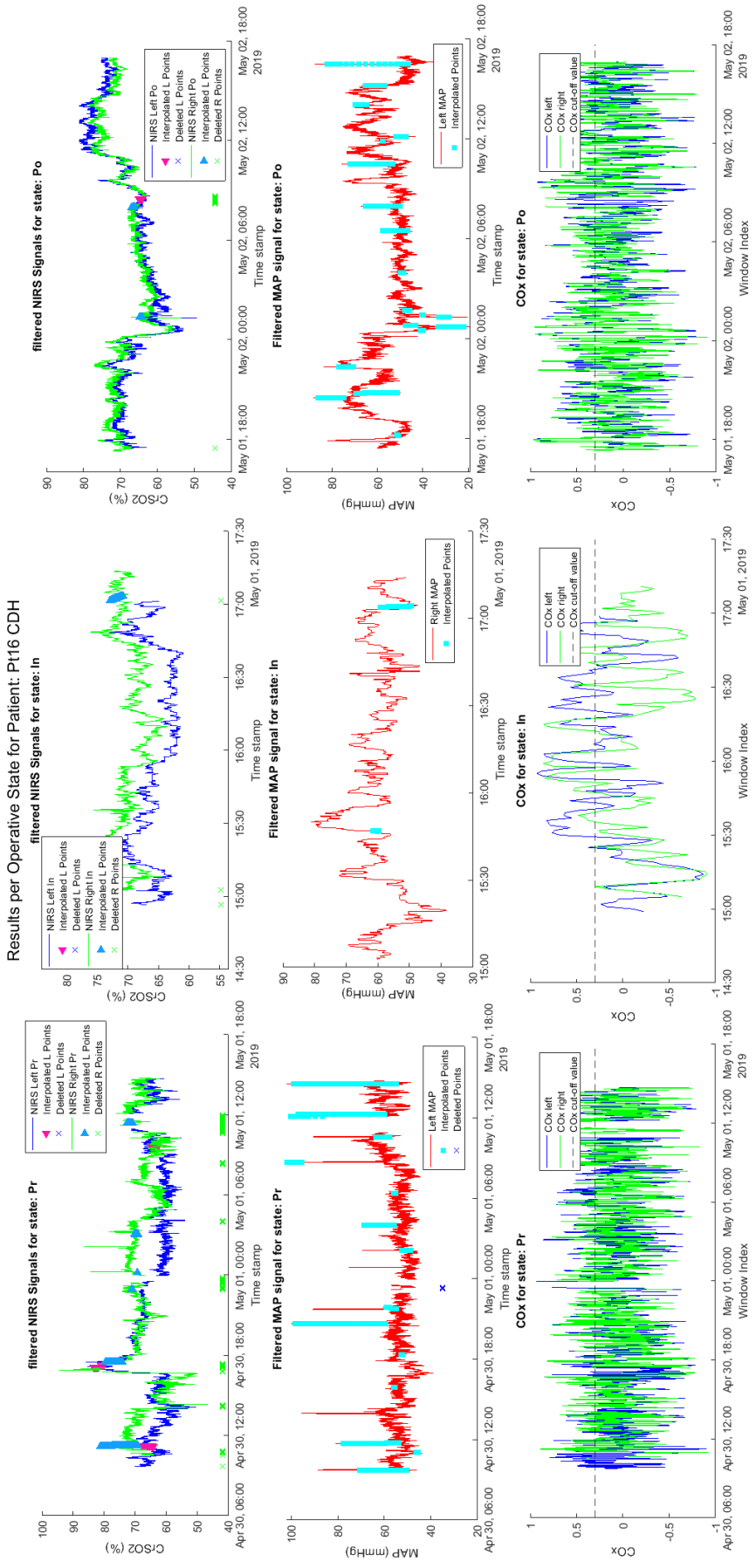

Figure 3.3: Preprocessed signals for MAP and $CrSO_2$ left and right with the resulting COx signal and cut-off value. Interpolated and deleted points in the signals are visualized.

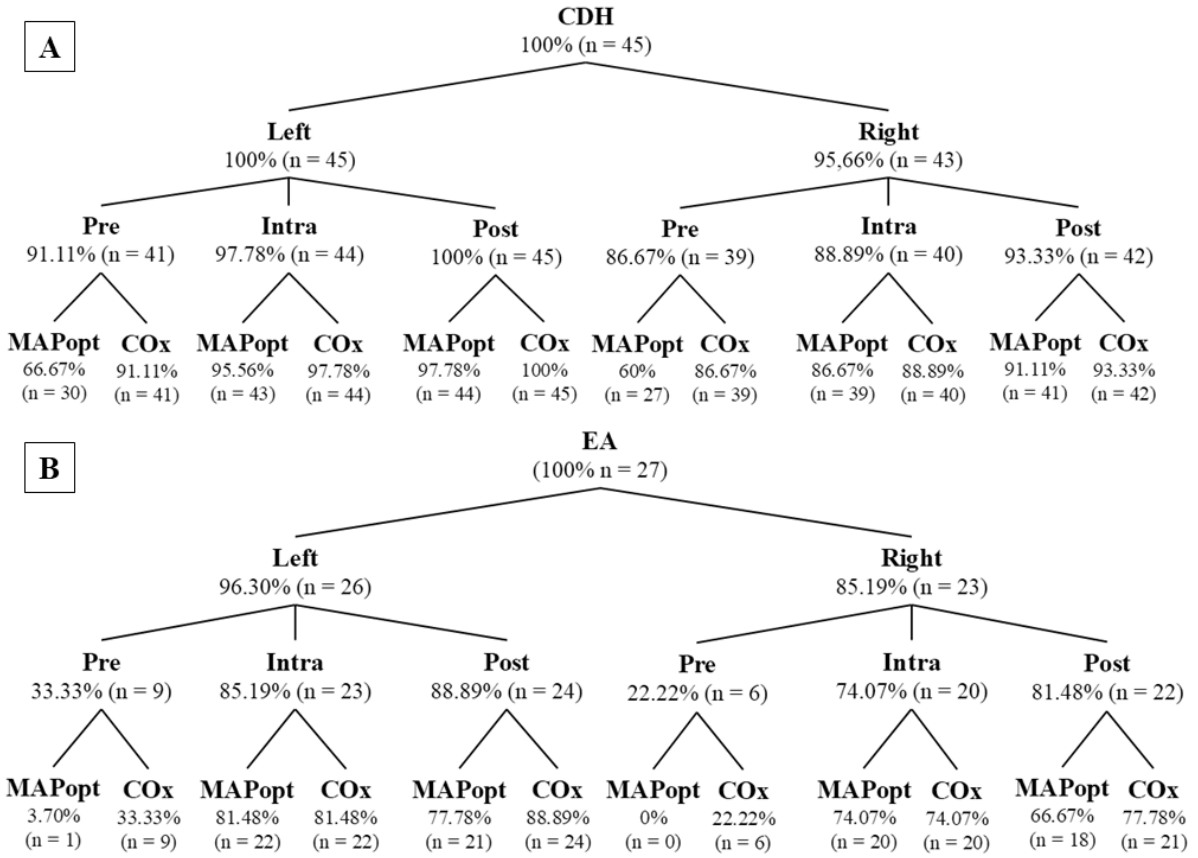

Figure 3.4: Overview of the data distribution for CDH (A) and EA (B) leading to the parameters derived with the algorithm developed in this study. (CDH = congenital diaphragmatic hernia, EA = Esophageal Atresia, COx = cerebral oximetry index, MAP_{opt} = optimal mean arterial pressure)

3.3. COx

The distributions and trends of mean COx values across the preoperative, intraoperative, and postoperative states for both CDH and EA patient groups are depicted in Figure 3.5A and 3.5B.

In the preoperative window, mean COx values are relatively low for both patient groups, with a narrow IQR. As the patients move into the intraoperative window, an increase in COx values is observed, particularly in the EA group, where COx values are consistently higher compared to the CDH group. The intraoperative period displays a broader distribution of COx values. Following surgery, in the postoperative window, COx values for both groups decrease, returning to levels comparable to those seen preoperatively. The postoperative distributions are also similar to preoperative values, with comparable IQRs in both patient groups.

Overall, COx values peak during the intraoperative window and then decline postoperatively for both groups, with the trend being more pronounced in the EA group.

COx Above Cut-Off Value

The percentage of time during which the COx exceeded the cut-off value of 0.3 was calculated for all segments where COx data was successfully derived (Fig. 3.4). The distribution and trends in these percentages across preoperative, intraoperative, and postoperative states for both CDH and EA patient groups are presented in Figure 3.5C and 3.5D.

The intraoperative state consistently exhibited a broader distribution of the percentage of time during which COx exceeded 0.3 for both patient groups. In the preoperative window, the percentage of time above the COx cut-off was lower for the EA group compared to the CDH group. During the intraoperative window this percentage increased for both groups, with the EA group showing a higher

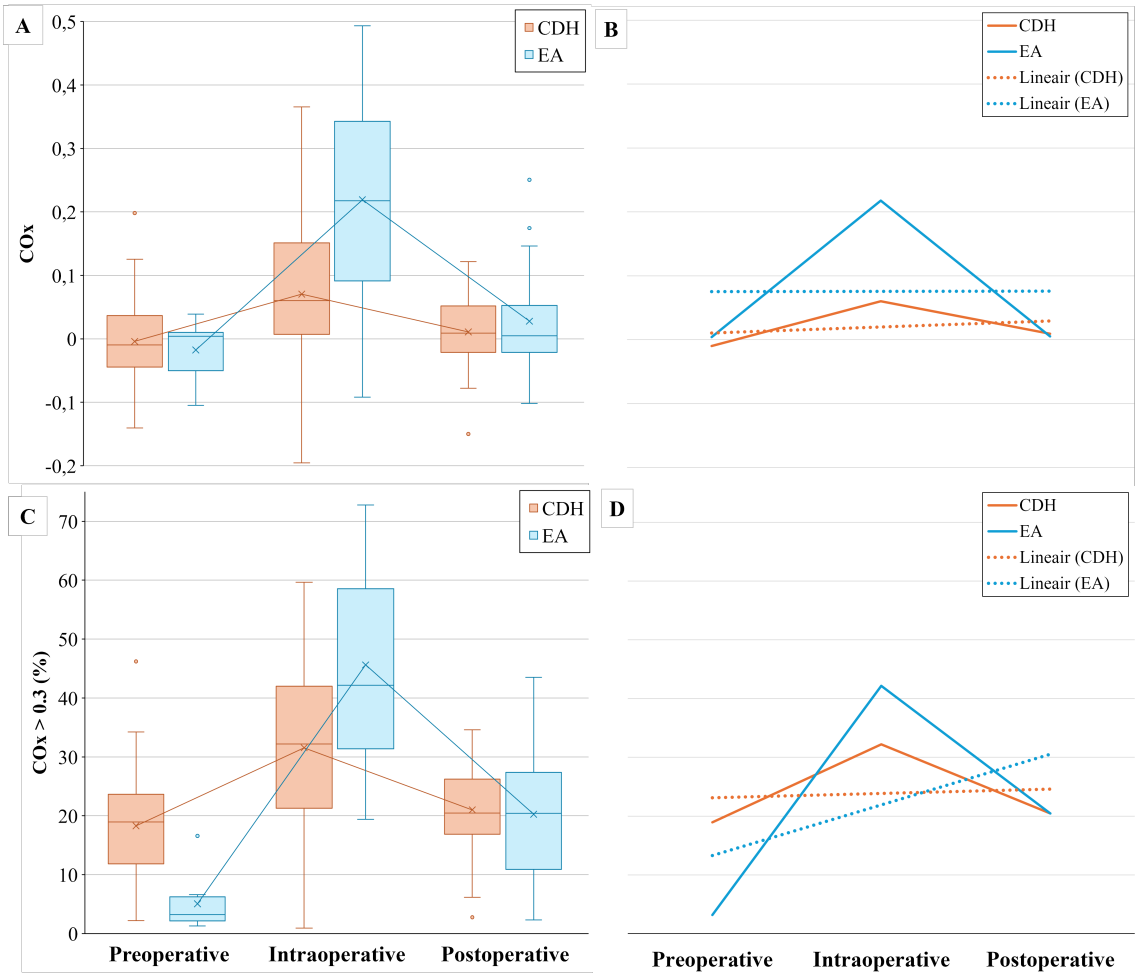

Figure 3.5: Boxplots illustrating the distribution (A) and median trends (B) of mean COx values for each operative state in the CDH and EA patient groups. Additionally, boxplots showing the distribution (C) and median trends (D) of the percentage of time that COx exceeded the cut-off value of 0.3 across the operative states for both patient groups. (CDH = Congenital Diaphragmatic Hernia, EA = Esophageal Atresia, COx = Cerebral Oximetry Index)

mean percentage and a broader range compared to the CDH group. Postoperatively, the percentage of time COx exceeded the cut-off value declined for both patient groups, returning to levels similar to those observed preoperatively.

Both groups exhibited similar trends, with an increase during the intraoperative period followed by a decline in the postoperative state. The trend was more pronounced in the EA group, with a higher peak intraoperatively followed by a sharper decline postoperatively.

3.4. MAP_{opt}

The MAP_{opt} was determined from the continuous COx signals for both patient groups, with successful identification in 89.24% of cases in the CDH group and 80.39% in the EA group. Figure 3.6 illustrates the MAP_{opt}-COx curve for an individual patient, highlighting how the nadir of the fitted curve represents MAP_{opt}. Notably, some fitted curves did not open upward, particularly in the intraoperative and postoperative phases, resulting in MAP_{opt} being determined at the beginning or end of the curve.

The distribution of MAP_{opt} values across the preoperative, intraoperative, and postoperative phases for both groups is presented in Figure 3.7A. The EA group showed limited preoperative data, with MAP_{opt} being determined in only one case. The CDH group exhibited consistent distributions across the operative phases, whereas the EA group showed greater variability in the intraoperative and postoperative phases.

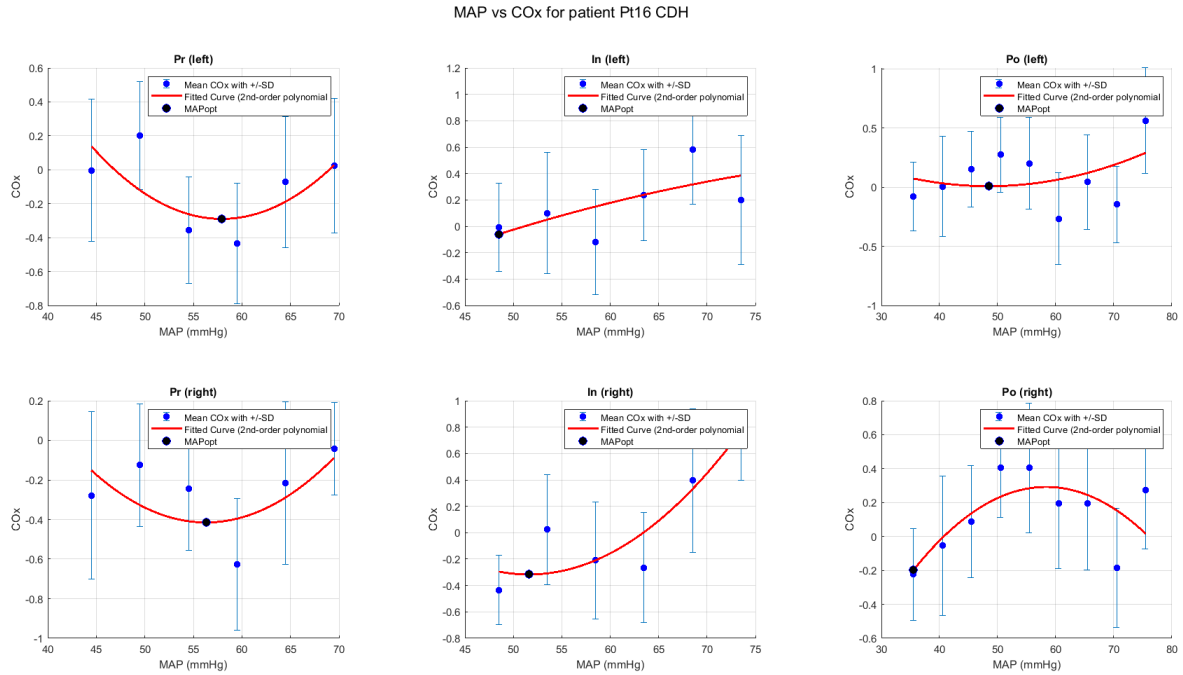

Figure 3.6: Fitted MAP-COx curve for a random individual patient, illustrating the relationship between mean arterial pressure (MAP) and the cerebral oximetry index (COx). The MAP_{opt} is represented as the nadir of the fitted curve.

Figure 3.7C illustrates the distribution of COx values corresponding to MAP_{opt} across the operative windows. Similar distributions were observed between the CDH and EA groups during the intra- and postoperative phases. Mean COx values at MAP_{opt} were higher for the EA group compared to the CDH group.

The trends in MAP_{opt} and COx at MAP_{opt} across operative windows are shown in Figures 3.7B and 3.7D respectively. MAP_{opt} demonstrated a trend opposite to that seen in COx, decreasing from the preoperative to intraoperative window and increasing postoperatively for both groups. Meanwhile, COx values at MAP_{opt} peaked during the intraoperative phase, particularly for the EA group. The CDH group, on the other hand, exhibited more consistent COx values at MAP_{opt} across all operative phases.

3.5. $CrSO_2$ sides (left/right)

The left and right $CrSO_2$ signals are analyzed separately to assess any potential differences in CA between hemispheres. The results show that there are no visually discernible differences between the left and right hemispheres across all operative windows and patient groups.

To demonstrate this, similar figures are generated for each parameter (mean COx, percentage COx above cut-off, MAP_{opt}, and COx at MAP_{opt}) using the left and right $CrSO_2$ signals independently. These figures are available in Appendix A.5. A visual examination of these plots did not reveal any notable discrepancies between the left and right $CrSO_2$ signals.

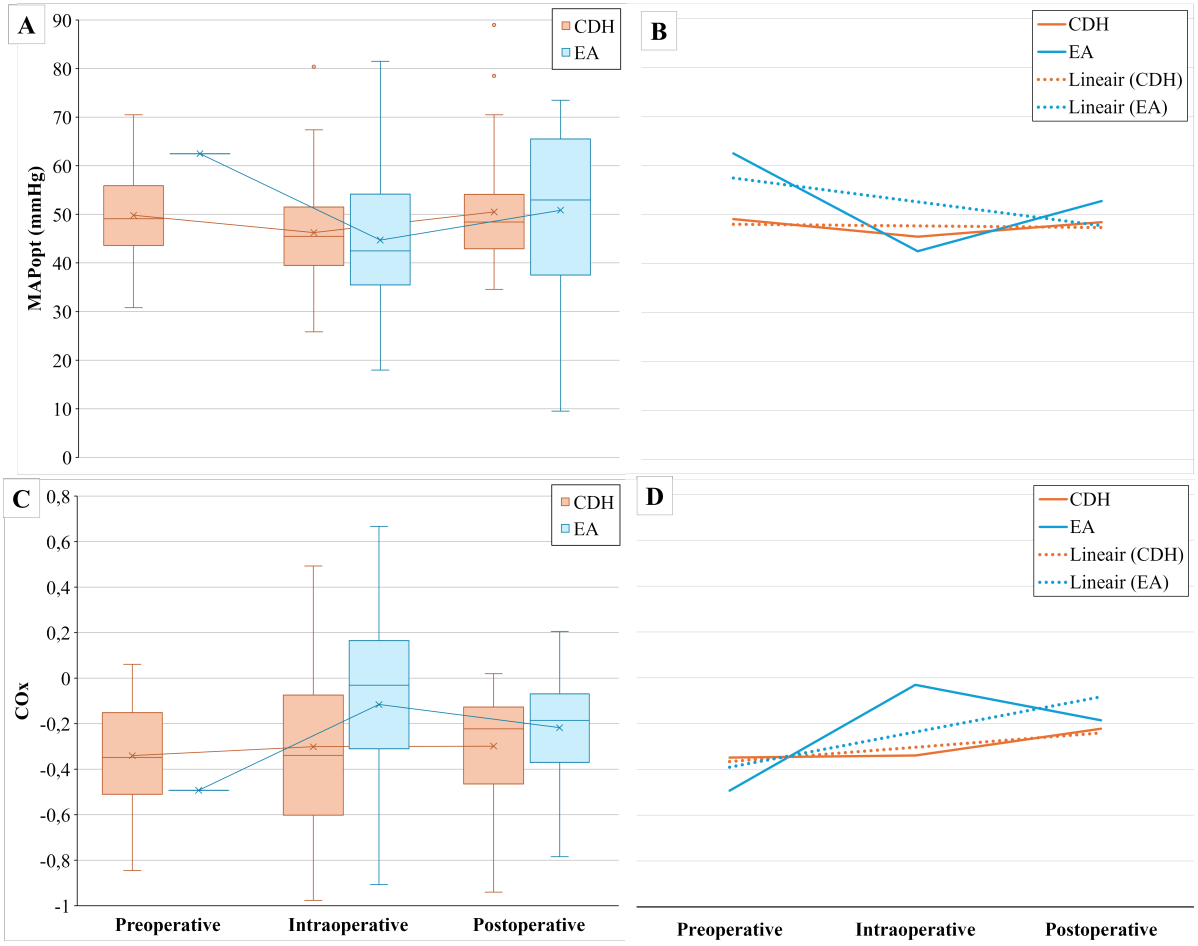

Figure 3.7: Boxplots illustrating the distribution (A) and median trends (B) of mean MAP_{opt} values for each operative state in the CDH and EA patient groups. Additionally, boxplots showing the distribution (C) and median trends (D) of the COx values at the MAP_{opt} across the operative states for both patient groups. (CDH = Congenital Diaphragmatic Hernia, EA = Esophageal Atresia, COx = Cerebral Oximetry Index)

4

Discussion

The goal of this study was to determine the feasibility of using the COx, derived from $CrSO_2$ and MAP signals, in order to identify the MAP_{opt} for effective CA in pediatric patients undergoing CDH or EA surgeries and to assess potential difference in CA between the three operative states.

COx trends across operative states demonstrated that both patient groups experienced a difference in COx values during the intraoperative period as expected. Intraoperatively the COx trends peaked, after which they postoperatively declined again (Fig. 3.5). This suggests a reduced CA capacity during surgery, especially pronounced in EA patients, indicating potentially greater cerebral vulnerability during the intraoperative phase.

The MAP_{opt}, was successfully determined in the majority of cases (89.24% for CDH, 80.39% for EA), and trends in MAP_{opt} also showed a difference in the intraoperatively phase; a decrease intraoperatively and postoperatively a stabilization to the preoperative value, indicating a shift in optimal hemodynamic requirements based on surgical phase (Fig. 3.7).

Additionally, the EA group exhibited higher intraoperative COx values and a lower MAP_{opt} compared to the CDH group. The percentage of time with COx above the cut-off value of 0.3, indicating impaired CA, was found to be highest during the intraoperative state for both groups, specifically for EA patients, suggesting differences in hemodynamic needs between these populations. COx values at MAP_{opt} were typically beneath the cut-off value of 0.3 (Fig. 3.7C and D), supporting its potential as a clinical target for optimizing CA during surgery.

4.1. COx and MAP_{opt}

The analysis of COx trends revealed distinct patterns across the pre-, intra-, and postoperative windows for both patient groups. In general, COx values tended to peak during the intraoperative state, suggesting a decrease in CA capacity during surgery. This trend suggests that surgical intervention imposes a strain on CA, which may gradually recover during the postoperative period.

Anesthesia

In the CDH group, anesthesia was provided with a continuous inhaled sevoflurane bolus of fentanyl and rocuronium [18]. MAP significantly decreases after sevoflurane induction in children older than two, yet CBFV remains constant, suggesting intact CA capacity in older patients [17]. However, Jildenstal et al. found that cerebral perfusion can become pressure-dependent during sevoflurane anesthesia in the youngest pediatric patients, indicating restricted effectiveness of cerebral blood flow autoregulation [16]. Further supporting this, Rhondali et al. demonstrated that a 20% drop in MAP led to a substantial drop in CBFV in infants under six months, measured using transcranial Doppler [15].

If a decrease in MAP due to sevoflurane administration coincides with an increase in COx, this indicates compromised CA. The resulting higher COx value reflects an increased dependency of $CrSO_2$ on MAP, implying that fluctuations in systemic blood pressure are directly affecting cerebral

oxygenation. This weakened ability to maintain stable $CrSO_2$ levels, particularly when MAP falls, suggests impaired cerebral perfusion. These findings highlight the vulnerability of younger infants' CA during anesthesia and surgery, which aligns with the observed intraoperative increase in COx trends in this study. Specifically, the restricted effectiveness of CA under sevoflurane anesthesia, as indicated by the sensitivity of cerebral perfusion to MAP changes, suggests that elevated COx values in CDH patients during the intraoperative phase may be attributable to anesthesia-induced impairment of CA. This alignment with prior research underscores the impact of sevoflurane on CA in young infants.

Hypercapnia

In addition to the effects of anesthesia, hypercapnia during neonatal surgery likely contributed to the observed intraoperative trends in COx. Hypercapnia, which involves elevating CO_2 levels to induce vasodilation, is commonly used to enhance CBF and oxygen delivery during neonatal surgeries [25]. Thoracoscopic procedures, such as the repair of EA and CDH, are particularly associated with intraoperative hypercapnia and acidosis due to CO_2 insufflation and absorption [26, 27]. McCulloch et al. have shown that even at relatively low concentrations of sevoflurane, hypercapnia can impair CA in healthy adults, with effects observed at a $PaCO_2$ of just 50 mmHg [28]. Hypercapnia promotes cerebral vasodilation, making CBF more dependent on systemic blood pressure, thereby reducing the brain's ability to regulate perfusion effectively during MAP fluctuations [25].

The observed increase in COx during hypercapnia suggests compromised CA, where $CrSO_2$ becomes more directly influenced by MAP changes. The elevated COx values observed intraoperatively, particularly in the EA group, suggest that hypercapnia impairs CA, increasing vulnerability during surgery. Mitigating hypercapnia through normocapnia may help preserve CA and improve the stability of MAP_{opt} during critical surgical procedures.

Clinical and Surgical Factors

The differences observed between CDH and EA patient groups in terms of COx and MAP_{opt} during the intraoperative phase can be attributed to their underlying clinical and surgical characteristics. CDH patients, who often require intensive preoperative stabilization due to respiratory issues like pulmonary hypoplasia, tend to have a relatively stable physiological state once optimized for surgery [29–32]. As a result, the transition into the surgical environment might not induce as significant a change in the physiological status of CDH patients compared to EA patients, leading to relatively stable intraoperative COx values. Their MAP_{opt} values also remained consistent, indicating that the stabilization measures were effective in maintaining optimal cerebral perfusion.

In contrast, while EA patients are also effectively stabilized preoperatively, they do not generally need the same intensive interventions as CDH patients. However, the intraoperative stress —whether related to anesthesia, hemodynamic fluctuations, or other surgical factors— might represent a relatively more significant physiological challenge for these patients. This increased vulnerability could explain the higher and more variable COx values during surgery, as their baseline physiological state is less compromised, making the impact of the surgical intervention more noticeable.

Next to this, EA patients face greater physiological challenges due to the nature of the thoracoscopic procedure, which requires lung displacement and often results in cardiorespiratory instability. This can lead to greater fluctuations in hemodynamics and causing hypercapnia for instance. This is reflected in the elevated and more variable intraoperative COx values observed in EA patients, indicating compromised CA. The higher and more variable MAP_{opt} values, as well as the increased COx at MAP_{opt}, suggest that maintaining optimal perfusion was more difficult for EA patients during the intraoperative period.

These findings highlight that both the type of preoperative stabilization and the specific demands of the surgical procedure could play roles in maintaining stable CA during surgery. This suggests a need for tailored intraoperative hemodynamic management to support CA, especially in surgeries that inherently disrupt thoracic or vascular stability.

MAPopt

MAP_{opt} was successfully determined in 89.24% of CDH patients and 80.39% of EA patients, with challenges primarily occurring during the preoperative window for EA patients due to limited MAP

variation (less than three MAP bins available). MAP_{opt} values were generally lower intraoperatively compared to pre- and postoperative periods, suggesting a shift in the MAP_{opt} needed to maintain CA during surgery. This decrease in MAP_{opt} is consistent with the elevated COx values observed intraoperatively, implying that the ability to maintain stable CA becomes more challenging during surgery, and therefore, the MAP_{opt} shifts to accommodate the reduced CA capacity.

During the intraoperative state, both patient groups experienced a reduction in MAP_{opt}, which could be reflecting the effects of anesthesia, surgical manipulation, and reduced systemic vascular resistance. This lower MAP_{opt}, coupled with increased COx values, emphasizes the importance of managing MAP to maintain CA, as the MAP_{opt} for effective CA shifts downward under surgical conditions. In the postoperative state, MAP_{opt} increased again, aligning with a reduction in COx, which suggests stabilization of hemodynamics and recovery of CA capacity as the effects of anesthesia and surgery diminished.

COx values at MAP_{opt} were generally low, indicating effective CA at the MAP_{opt} in most cases. However, during the intraoperative phase, COx values at MAP_{opt} sometimes exceeded 0.3, suggesting that even when MAP was maintained within the "optimal" range, CA was still compromised. This indicates that the ideal MAP_{opt} may vary dynamically, and factors such as anesthesia, hypercapnia, and surgical stress can influence whether CA remains intact even at this presumed optimal MAP.

Comparison Between Left and Rigth Hemispheres

The comparison between the left and right $CrSO_2$ signals revealed no big differences in the COx trends or MAP_{opt} values across the three operative states (Appendix A.5). Both hemispheres exhibited similar patterns in COx and MAP_{opt}, suggesting homogeneity in cerebral perfusion during and after surgery for both CDH and EA patient groups.

The absence of observable differences between the left and right hemispheres might indicate that the surgical procedures did not differentially affect cerebral perfusion in either hemisphere. Additionally, the surgical positioning and approach likely ensured a consistent systemic impact on blood flow and cerebral oxygenation, thereby resulting in similar perfusion patterns on both sides. This finding aligns with the assumption that, in the absence of focal injuries or specific interventions that may affect one hemisphere more than the other, systemic factors such as blood pressure and ventilation affect both hemispheres in a relatively balanced manner [4].

4.2. Validity of COx as CA Metric

The findings of this study demonstrate that COx trends across the pre-, intra-, and postoperative phases align with what is known about CA physiology. In particular, the intraoperative increase in COx values coincides with periods when CA can be expected to be impaired, such as during anesthesia and hypercapnia, suggesting that COx could be an effective tool for identifying reduced autoregulatory capacity under these conditions. This consistency between the observed COx trends and known physiological responses to surgical stress and anesthesia adds credibility to the use of COx as a surrogate marker for CA.

However, it is important to acknowledge the interdependent relationship between COx as a metric and the CA behavior observed in this study. This relationship raises an inherent question: Is COx a reliable measure of CA because its trends align with what is physiologically expected, or is the physiological conclusion about CA during surgery shaped by the way COx behaves? This highlights a potential limitation in relying solely on COx as a measure of CA.

Moreover, the explanations provided in this study for why CA might be compromised during different operative states are primarily based on reasoning from literature and existing knowledge rather than direct measurement. This means that, while the findings align logically with what is known about the physiological effects of surgery, anesthesia, and hypercapnia on CA, the actual mechanisms leading to impaired CA in these specific patient groups were not directly investigated.

To avoid circular reasoning, it is crucial to interpret the findings in the context of existing knowledge on CA and surgical interventions. The observed increase in COx during the intraoperative phase supports the notion that CA could be compromised under surgical stress, hypercapnia, and anesthesia. Rather

than proving the validity of COx solely by the trends observed in this study, the findings should be seen as being in logical agreement with previous literature on CA in young infants. This logical congruence strengthens the use of COx as a surrogate for CA.

4.3. Limitations

Measurement and Analysis Constraints

It is challenging to directly attribute observed COx values to specific physiological mechanisms. While suggested that anesthesia, hypercapnia, and thoracoscopic procedures might explain the intraoperative rise in COx, these factors were not directly measured. The proposed explanations are based on literature and general physiological reasoning.

NIRS

The use of NIRS as a method to assess cerebral oxygenation in this study provides a practical and non-invasive approach, but also presents some limitations that could have influenced the results. Factors such as signal attenuation due to skull thickness, variations in tissue path length, and insufficient slow-wave power may have affected the precision of $CrSO_2$ measurements [4]. These factors could impact COx calculations and potentially lead to under- or overestimation of CA. Furthermore, while NIRS cannot directly measure CPP or CBF, making it less comprehensive compared to invasive methods, its ability to capture changes in cerebral oxygenation offers a promising window into the functioning of CA. The consistency of findings across patients might suggest that the impact of such factors was not of high significance.

MAP_{opt} Determination

Determining MAP_{opt} was successful in most patients but was challenging in others, particularly during the preoperative window in the EA group. When the range of the MAP signal was insufficient to create the necessary MAP bins, MAP_{opt} could not be accurately determined, which may have influenced some of the intraoperative CA findings. In cases where the fitted MAP_{opt}-COx curve did not open upward, the determination of the nadir was not clear, which may have also led to incorrect MAP_{opt} values.

Generalizability

The results of this study are limited to the specific population of neonates with CDH or EA admitted to a single PICU. As such, the findings may not be generalizable to other populations. Additionally, the physiological characteristics of neonates, particularly their CA mechanisms, differ from those of older children, meaning the insights gained here may not be applicable to a broader population.

Study Design and Data Limitations

The dataset used was subject to data incompleteness, with missing data for certain operative states and individual patients. For instance, the absence of bilateral NIRS data in a subset of patients limited the ability to perform comprehensive analyses of hemispheric differences. Additionally, the purely observational design and the relatively small cohort size impaired the power, which might have limited the ability to detect smaller but clinically relevant differences. These aspects, combined with potential biases introduced by patient selection, restrict the overall generalizability of the findings.

Data Completeness and Preprocessing Limitations

Data completeness differed significantly between the CDH and EA groups, with only 22% of EA patients having data for all operative states compared to 82% for CDH patients. Inconsistent bilateral NIRS data and limited preoperative data might have constrained comprehensive analysis of CA.

Preprocessing led to some data loss: 10% of NIRS and 5% of MAP signals were interpolated, while 15% of NIRS and 5% of MAP data were deleted. While linear interpolation and filtering methods helped maintain signal continuity, they may have introduced inaccuracies, impacting the assessment of CA trends across the perioperative period. However, the preprocessing process was designed to make this impact as low as possible.

4.4. Implications for Clinical Practice

COx Analysis

The trends observed in COx across the different operative windows indicate that CA (CA) is most compromised during the intraoperative period for both the CDH and EA patient groups. The elevation in COx values during this phase, particularly for EA patients, suggests a heightened vulnerability in maintaining stable cerebral perfusion during surgical interventions. This highlights the critical importance of vigilant hemodynamic monitoring and intervention during the intraoperative period.

The elevated intraoperative COx values in EA patients underscore the need for tailored approaches to hemodynamic management, as these patients appear to experience more significant disruptions in CA. This could potentially necessitate a more aggressive intervention strategy to maintain optimal cerebral perfusion, such as more frequent adjustments in vasopressor support or fluid management during surgery. Implementing individualized interventions based on real-time COx values could potentially help mitigate the risk of impaired CA and thereby reduce the likelihood of adverse neurological outcomes in these vulnerable patients.

The differences observed between the CDH and EA groups emphasize the need for tailored hemodynamic management strategies, accounting for the unique susceptibilities of each group. For instance, EA patients may require a more proactive approach to maintaining stable CA, while CDH patients could potentially benefit from focused perioperative monitoring to ensure they remain within optimal hemodynamic ranges.

MAP_{opt}

The findings of this study emphasize the potential utility of individualized MAP targets in the perioperative care of pediatric patients undergoing CDH or EA repair. The identification of MAP_{opt} provides a clinically relevant target that can help guide interventions to optimize cerebral perfusion, particularly during the vulnerable intraoperative period. Maintaining MAP within the individualized MAP_{opt} range could potentially help to reduce the risk of impaired CA and improve neurological outcomes.

However, the variability in COx values at MAP_{opt} observed in this study underscores the importance of taking a comprehensive approach to hemodynamic management. MAP_{opt} represents the pressure at which CA is retrospectively most effective, but the effectiveness of CA at these MAP levels still varies between patients and across different operative states. This suggests the need for frequently and continuously updating the determination of the MAP_{opt} to ensure intact, particularly in patients with inherently compromised autoregulation.

Target MAP in Surgical Setting

The observed MAP_{opt} values in this study provide insight into the patient-specific MAP_{opt} that could potentially be targeted to optimize cerebral perfusion in neonates undergoing surgical repair of CDH or EA. However, there was notable variability in MAP_{opt} across patients and operative states, indicating that the optimal MAP target is not a fixed value but should be updated frequently. This approach aligns with the growing trend toward precision medicine, where hemodynamic targets are tailored to the specific needs of each patient based on real-time physiological data.

The intraoperative decrease in MAP_{opt} observed in both patient groups suggests that maintaining MAP within a lower range during surgery might be beneficial for optimizing CA. In contrast, postoperative increases in MAP_{opt} indicate a need to adjust MAP targets during recovery to maintain effective CA as physiological conditions change. These findings suggest that clinicians should aim to maintain MAP within a dynamically adjusted target range that considers both patient-specific factors and the operative context.

COx as Monitoring Tool

The results of this study provide promising leads for the use of COx as a marker of CA in pediatric patients undergoing surgery for CDH or EA. The clear trends observed in COx, particularly the intraoperative increase and subsequent postoperative decrease, highlight its utility in tracking CA status throughout the operative periods. COx provides real-time feedback on the relationship between

cerebral oxygenation and systemic blood pressure, which could be valuable for informing clinical decision-making and guiding hemodynamic interventions in the future.

However, the variability in COx values, even at MAP_{opt}, suggests that it may not be sufficient as a standalone measure. Instead, COx could be used in the future as part of a comprehensive hemodynamic monitoring approach, in conjunction with other physiological parameters, to provide a more complete picture of CA status. Future research should focus on validating COx as a reliable marker of CA in different patient populations and surgical settings, and on integrating COx into existing clinical workflows in a way that enhances decision-making without adding unnecessary complexity.

If thoroughly validated through further studies, COx could be recommended for routine use as a non-invasive measure of CA, helping to ensure that hemodynamic interventions are not only based on achieving target MAP values but also on maintaining effective cerebral perfusion. This approach has the potential to improve neurological outcomes by ensuring that CA is preserved throughout the operative period.

4.5. Future Research Directions

The findings of this study open several directions for future research aimed at further exploring the COx, validating MAP_{opt}-guided management and understanding the dynamics of CA in pediatric patients undergoing CDH or EA surgery. Below are suggested research directions organized in a logical sequence based on the next steps following this research keeping in mind the clinical achievability:

COx Validation

The logical congruence between the findings and the literature strengthens the use of COx as a surrogate for CA, but also underlines the need for continued validation through direct measurement of influencing factors (e.g., anesthesia, hypercapnia or surgical procedures). Future research should focus on measuring these factors directly to confirm their role in the intraoperative trends in COx observed in this study. This also underlines the need for continued validation through direct measurement of influencing factors. This means future studies are necessary to confirm these specific relationships. In the dataset used in this study, medication administration and patient and surgical characteristics are available which opens up this further research.

Incorporation of Neurological Outcomes

The results of this study already show that the CA stabilize postoperatively back to the preoperatively value after altering in the intraoperative phase suggesting stabilization of the CA after surgery. Postoperative neurological outcome data is however available in the dataset used for this study, no comparison has been made between MAP, distance from MAP_{opt}, and neurological outcomes. Future studies should focus on evaluating these relationships, as understanding how MAP_{opt}-guided management influences neurological outcomes would provide a more direct assessment of the clinical relevance of optimizing CA. This research could help determine whether maintaining MAP within individualized optimal ranges leads to better short-term and long-term neurological outcomes, thus justifying the use of MAP_{opt} in perioperative care.

Advanced Signal Processing and Preprocessing Refinements

A logical continuation would involve refining the preprocessing techniques applied to MAP and $CrSO_2$ signals. More advanced algorithms, such as machine learning-based interpolation or noise reduction, could be implemented to enhance data quality. By improving signal reliability, the accuracy of calculated COx and derived MAP_{opt} values can be further validated, ensuring more robust assessments of CA.

Keeping in mind the the clinical implication of the COx, the continuity of the COx signal should be included. The determination of the MAP_{opt} was done for the whole length of the COx signal but could also be calculated using a multi-window weighted algorithm [8]. Next, the ULA and LLA could also be determined to calculate the optimal MAP range instead of one point.

This study utilized a COx cut-off value of 0.3 to define impaired autoregulation. Future research should consider exploring alternative cut-off values, as it is possible that a different threshold may better reflect CA impairment in this population, particularly during surgery.

Quantitative Metrics

This study found no significant differences between left and right hemispheric $CrSO_2$ signals, but this conclusion was based on a primarily qualitative assessment. Future research should involve more complete bilateral data to explore hemispheric differences with greater accuracy. Using quantitative metrics, such as correlation analysis, statistical tests, and detailed time-series comparisons, could help identify any subtle variations between hemispheres during surgery and recovery. Understanding these potential differences could provide insight into focal injury, ischemia, or the differential effects of surgery and anesthesia, and could ultimately contribute to more targeted management of cerebral perfusion.

Validation of MAP_{opt} as a Clinical Target

To fully evaluate the potential benefits of MAP_{opt}-guided blood pressure management, prospective randomized trials are needed in a broader range of clinical settings and patient populations. Such trials would help determine if maintaining MAP at MAP_{opt} can consistently optimize cerebral perfusion and improve neurological outcomes during surgery. The variability observed in COx values at MAP_{opt} suggests that more evidence is required to validate these values as reliable clinical targets for optimizing CA in neonates undergoing surgical interventions.

COx Comparison with Other Cerebral Autoregulation Metrics

COx is one of several metrics that can be used to assess CA. While this study shows promising results, future research should aim to validate COx against other established markers, such as the pressure reactivity index (PRx), to evaluate its reliability more comprehensively. It may be beneficial to explore correlations between MAP_{opt}, COx, and other CA indices, such as the PRx, which is commonly used in invasive ICP monitoring settings. Investigating these correlations could help determine the reliability of NIRS-derived parameters, such as COx, compared to more established metrics. Although PRx requires invasive monitoring, it could provide valuable information when used alongside COx [4].

Longitudinal Analysis

Future research could also benefit from a longitudinal approach, tracking changes in COx, MAP_{opt}, and CA across multiple surgical interventions or over extended postoperative periods. Such studies could help elucidate how cerebral perfusion and autoregulatory function change throughout the course of a patient's treatment, from preoperative stabilization to long-term recovery. This would allow for a more dynamic understanding of CA in pediatric patients and the role that optimal MAP management plays in maintaining stable cerebral perfusion, especially in the context of repeated or extended surgical care.

5

Conclusion

This study demonstrates the feasibility of determining patient specific MAP_{opt} for maintaining effective CA in neonates undergoing surgery for CDH or EA, using the COx derived from NIRS. The findings indicate that CA, as reflected by COx, is most compromised during the intraoperative state as suspected and provide insights into the perioperative dynamics of CA in these patient populations. While the resulted COx trends align with current physiological understanding, the exact nature of the relationship between COx trends and CA impairment during surgery requires further investigation to confirm whether the observed COx behavior directly reflects true changes in CA capacity. This research provides an important step towards individualized hemodynamic management strategies for improving cerebral perfusion and outcomes in neonates undergoing critical surgical procedures.

Bibliography

1. Udomphorn, Y., Armstead, W. M. & Vavilala, M. S. Cerebral blood flow and autoregulation after pediatric traumatic brain injury. en. *Pediatr. Neurol.* **38,** 225–234 (Apr. 2008).
2. Pelizzo, G. *et al.* Pediatric laparoscopy and adaptive oxygenation and hemodynamic changes. en. *Pediatr. Rep.* **9,** 7214 (June 2017).
3. Yuki, K. *et al.* Pediatric perioperative stress responses and anesthesia. en. *Transl. Perioper. Pain Med.* **2,** 1–12 (2017).
4. Van den Boom, J. Advancements and Challenges in Assessing Cerebral Autoregulation in the Pediatric Intensive Care Unit (PICU): A Review of Methodologies, Applications, and Insights with a Focus on Near-Infrared Spectroscopy (NIRS) (2024).
5. Weber, F. & Scoones, G. P. A practical approach to cerebral near-infrared spectroscopy (NIRS) directed hemodynamic management in noncardiac pediatric anesthesia. en. *Paediatr. Anaesth.* **29,** 993–1001 (Oct. 2019).
6. Kurz, J. E., Smith, C. M. & Wainwright, M. S. Thermoregulate, autoregulate and ventilate: brain-directed critical care for pediatric cardiac arrest. en. *Curr. Opin. Pediatr.* **29,** 259–265 (June 2017).
7. Rivera-Lara, L. *et al.* Near-infrared spectroscopy-derived cerebral autoregulation indices independently predict clinical outcome in acutely ill comatose patients. en. *J. Neurosurg. Anesthesiol.* **32,** 234–241 (July 2020).
8. Kirschen, M. P. *et al.* Deviations from NIRS-derived optimal blood pressure are associated with worse outcomes after pediatric cardiac arrest. en. *Resuscitation* **168,** 110–118 (Nov. 2021).
9. Abecasis, F., Dias, C., Zakrzewska, A., Oliveira, V. & Czosnyka, M. Monitoring cerebrovascular reactivity in pediatric traumatic brain injury: comparison of three methods. en. *Childs. Nerv. Syst.* **37,** 3057–3065 (Oct. 2021).
10. Bush, B., Sam, K. & Rosenblatt, K. The role of near-infrared spectroscopy in cerebral autoregulation monitoring. en. *J. Neurosurg. Anesthesiol.* **31,** 269–270 (July 2019).
11. Lee, J. K. *et al.* Cerebrovascular autoregulation in pediatric moyamoya disease. en. *Paediatr. Anaesth.* **23,** 547–556 (June 2013).
12. Zipfel, J. *et al.* Identifying the optimal blood pressure for cerebral autoregulation in infants after cardiac surgery by monitoring cerebrovascular reactivity-A pilot study. en. *Paediatr. Anaesth.* **32,** 1320–1329 (Dec. 2022).
13. Lally, K. P. *et al.* Standardized reporting for congenital diaphragmatic hernia–an international consensus. en. *J. Pediatr. Surg.* **48,** 2408–2415 (Dec. 2013).
14. Hendrikx, D., Van Huffel, S., Naulaers, G. & Caicedo Dorado, A. *Applications of Network Physiology in Neonatology* eng. 2021-12-13.
15. Rhondali, O. *et al.* Impact of sevoflurane anesthesia on cerebral blood flow in children younger than 2 years. en. *Paediatr. Anaesth.* **23,** 946–951 (Oct. 2013).
16. Jildenstål, P., Widarsson Norbeck, D., Snygg, J., Ricksten, S.-E. & Lannemyr, L. Cerebral autoregulation in infants during sevoflurane anesthesia for craniofacial surgery. en. *Paediatr. Anaesth.* **31,** 563–569 (May 2021).
17. Fairgrieve, R., Rowney, D. A., Karsli, C. & Bissonnette, B. The effect of sevoflurane on cerebral blood flow velocity in children. en. *Acta Anaesthesiol. Scand.* **47,** 1226–1230 (Nov. 2003).
18. Costerus, S. A. *et al.* Cerebral oxygenation and activity during surgical repair of neonates with congenital diaphragmatic hernia: A center comparison analysis. en. *Front. Pediatr.* **9,** 798952 (Dec. 2021).

19. Scholkmann, F., Spichtig, S., Muehlemann, T. & Wolf, M. How to detect and reduce movement artifacts in near-infrared imaging using moving standard deviation and spline interpolation. en. *Physiol. Meas.* **31,** 649–662 (May 2010).

20. NHSGGC. *NIRS guidelines 2021* Nov. 2021. `https://www.clinicalguidelines.scot.nhs.uk/nhsggc-guidelines/nhsggc-guidelines/anaesthetics/near-infrared-spectroscopy-nirs-guideline/`.

21. Hirsch, J. C., Charpie, J. R., Ohye, R. G. & Gurney, J. G. Near-infrared spectroscopy: what we know and what we need to know–a systematic review of the congenital heart disease literature. en. *J. Thorac. Cardiovasc. Surg.* **137,** 154–9, 159e1–12 (Jan. 2009).

22. Swarte, R. *Near-Infrared Spectroscopy (NIRS) neuromonitoring (Versie 1)* (eds de Jonge, R. & Reiss, I.)

23. Fraser 3rd, C. D. *et al.* The frequency response of cerebral autoregulation. en. *J. Appl. Physiol.* **115,** 52–56 (July 2013).

24. Aries, M. J. H. *et al.* Continuous determination of optimal cerebral perfusion pressure in traumatic brain injury. en. *Crit. Care Med.* **40,** 2456–2463 (Aug. 2012).

25. Kaiser, J. R., Gauss, C. H. & Williams, D. K. The effects of hypercapnia on cerebral autoregulation in ventilated very low birth weight infants. en. *Pediatr. Res.* **58,** 931–935 (Nov. 2005).

26. Pierro, A. Hypercapnia and acidosis during the thoracoscopic repair of oesophageal atresia and congenital diaphragmatic hernia. en. *J. Pediatr. Surg.* **50,** 247–249 (Feb. 2015).

27. Bishay, M. *et al.* Hypercapnia and acidosis during open and thoracoscopic repair of congenital diaphragmatic hernia and esophageal atresia: results of a pilot randomized controlled trial. en. *Ann. Surg.* **258,** 895–900 (Dec. 2013).

28. McCulloch, T. J., Visco, E. & Lam, A. M. Graded hypercapnia and cerebral autoregulation during sevoflurane or propofol anesthesia. en. *Anesthesiology* **93,** 1205–1209 (Nov. 2000).

29. Longoni, M., Pober, B. R. & High, F. A. en. in *GeneReviews(®)* (University of Washington, Seattle, Seattle (WA), 1993).

30. Williams, E. & Greenough, A. Respiratory support of infants with congenital diaphragmatic hernia. en. *Front. Pediatr.* **9,** 808317 (Dec. 2021).

31. Novotny, A. M. The use of inhaled nitric oxide in congenital diaphragmatic hernia. en. *Adv. Neonatal Care* **20,** 479–486 (Dec. 2020).

32. *Extracorporeal Life Support: The ELSO Red Book* 1st ed. English (eds Brogan, T., Lequier, L., Lorusso, R., MacLaren, G. & Peek, G.) ISBN: 978-0-9656756-5-9 (Extracorporeal Life Support Organization, May 2017).

A

Additional Results

A.1. Data Completeness Overview

Table A.1: Percentage of NaNs in the mean arterial pressure (MAP) signals before preprocessing for each operative state. Values are represented as median [IQR]. (CDH = Congenital Diaphragmatic Hernia, EA = Esophageal Atresia)

	CDH	**EA**
Preoperative NaN% MAP	0.93% [0.56 - 1.65]	0.87% [0.00 - 17.39]
Intraoperative NaN% MAP	6.56% [2.64 - 13.56]	29.41% [19.04 - 32.42]
Postoperative NaN% MAP	1.47% [0.93 - 2.25]	20.3% [0.95 - 8.16]

Table A.2: Percentage of NaNs in the $CrSO_2$ signals before preprocessing for each side and operative state. Values are represented as median [IQR]. (CDH = Congenital Diaphragmatic Hernia, EA = Esophageal Atresia)

	CDH	**EA**
Preoperative Left NaN% $CrSO_2$	1.64% [0.01 - 5.99]	0.56% [0.14 - 17.19]
Intraoperative Left NaN% $CrSO_2$	1.95% [0.08 - 12.44]	21.56% [0.00 - 47.36]
Postoperative Left NaN% $CrSO_2$	2.65% [0.45 - 10.04]	4.99% [2.65 - 14.61]
Preoperative Right NaN% $CrSO_2$	6.21% [0.76 - 15.90]	9.03% [2.70 - 17.98]
Intraoperative Right NaN% $CrSO_2$	0.41% [0.00 - 4.64]	0.31% [0.04 - 7.45]
Postoperative Right NaN% $CrSO_2$	2.54% [0.20 - 10.58]	0.22% [0.00 - 1.76]

Table A.3: Percentage of deleted and interpolated datapoints in the mean arterial pressure (MAP) signals for each operative state. Note: The percentage is calculated of the total of NaNs minus the NaN values in the beginning or ending of the signal. Values are represented as median [IQR]. (CDH = Congenital Diaphragmatic Hernia, EA = Esophageal Atresia)

	CDH		**EA**	
	% Deleted	**% Interpolated**	**% Deleted**	**% Interpolated**
Preoperative MAP	0.00% [0.00 - 0.04]	0.56% [0.29 - 0.98]	0.00% [0.00 - 7.98]	0.00% [0.00 - 0.21]
Intraoperative MAP	0.00% [0.00 - 4.33]	1.95% [0.66 - 2.87]	0.00% [0.00 - 4.87]	2.38% [1.59 - 2.98]
Postoperative MAP	0.00% [0.00 - 0.95]	0.80% [0.60 - 1.07]	0.54% [0.00 - 1.73]	0.93% [0.46 - 1.32]

Table A.4: Percentage of deleted and interpolated datapoints in the $CrSO_2$ signals for each operative state and side. Note: The percentage is calculated of the total of NaNs minus the NaN values in the beginning or ending of the signal. Values are represented as median [IQR]. (CDH = Congenital Diaphragmatic Hernia, EA = Esophageal Atresia)

	CDH		EA	
	% Deleted	**% Interpolated**	**% Deleted**	**% Interpolated**
Preoperative Left	0.00% [0.00 - 1.28]	0.00% [0.00 - 0.35]	0.00% [0.00 - 0.00]	0.28% [0.00 - 0.97]
Intraoperative Left	0.00% [0.00 - 3.32]	0.05% [0.00 - 0.43]	11.24% [0.00 - 53.51]	0.00% [0.00 - 0.71]
Postoperative Left	0.00% [0.00 - 0.00]	0.31% [0.00 - 2.05]	0.00% [0.00 - 6.15]	0.15% [0.00 - 0.91]
Preoperative Right	0.00% [0.00 - 3.25]	0.67% [0.00 - 1.70]	0.00% [0.00 - 6.15]	0.36% [0.22 - 1.57]
Intraoperative Right	0.00% [0.00 - 1.69]	0.00% [0.00 - 0.00]	0.00% [0.00 - 3.97]	0.07% [0.00 - 0.50]
Postoperative Right	0.00% [0.00 - 3.96]	0.03% [0.00 - 0.39]	0.00% [0.00 - 0.00]	0.00% [0.00 - 0.05]

Table A.5: Data availability of the $CrSO_2$ signals after preprocessing. Values are represented as % (n). (CDH = Congenital Diaphragmatic Hernia, EA = Esophageal Atresia)

	CDH (n=45)	**EA (n=27)**
Three states	82.22% (n=37)	22.22% (n=6)
Two states	11.11% (n=5)	48.15% (n=13)
One state	0.00% (n=0)	14.81% (n=4)
Only Left $CrSO_2$	0.00% (n=0)	14.81% (n=4)
Only Right $CrSO_2$	4.44% (n=2)	3.70% (n=1)

Table A.6: Data availability of the $CrSO_2$ signals after preprocessing for each state and each side. Values are represented as % (n). (CDH = Congenital Diaphragmatic Hernia, EA = Esophageal Atresia)

	CDH (n=45)	**EA (n=27)**
Preoperative Left $CrSO_2$	91.11% (n=41)	33.33% (n=9)
Intraoperative Left $CrSO_2$	97.78% (n=44)	85.19% (n=23)
Postoperative Left $CrSO_2$	100.00% (n=45)	88.89% (n=24)
Preoperative Right $CrSO_2$	86.67% (n=39)	22.22% (n=6)
Intraoperative Right $CrSO_2$	88.89% (n=40)	74.07% (n=20)
Postoperative Right $CrSO_2$	93.33%(n=42)	81.48% (n=22)

A.2. Detailed Preprocessing Pipeline

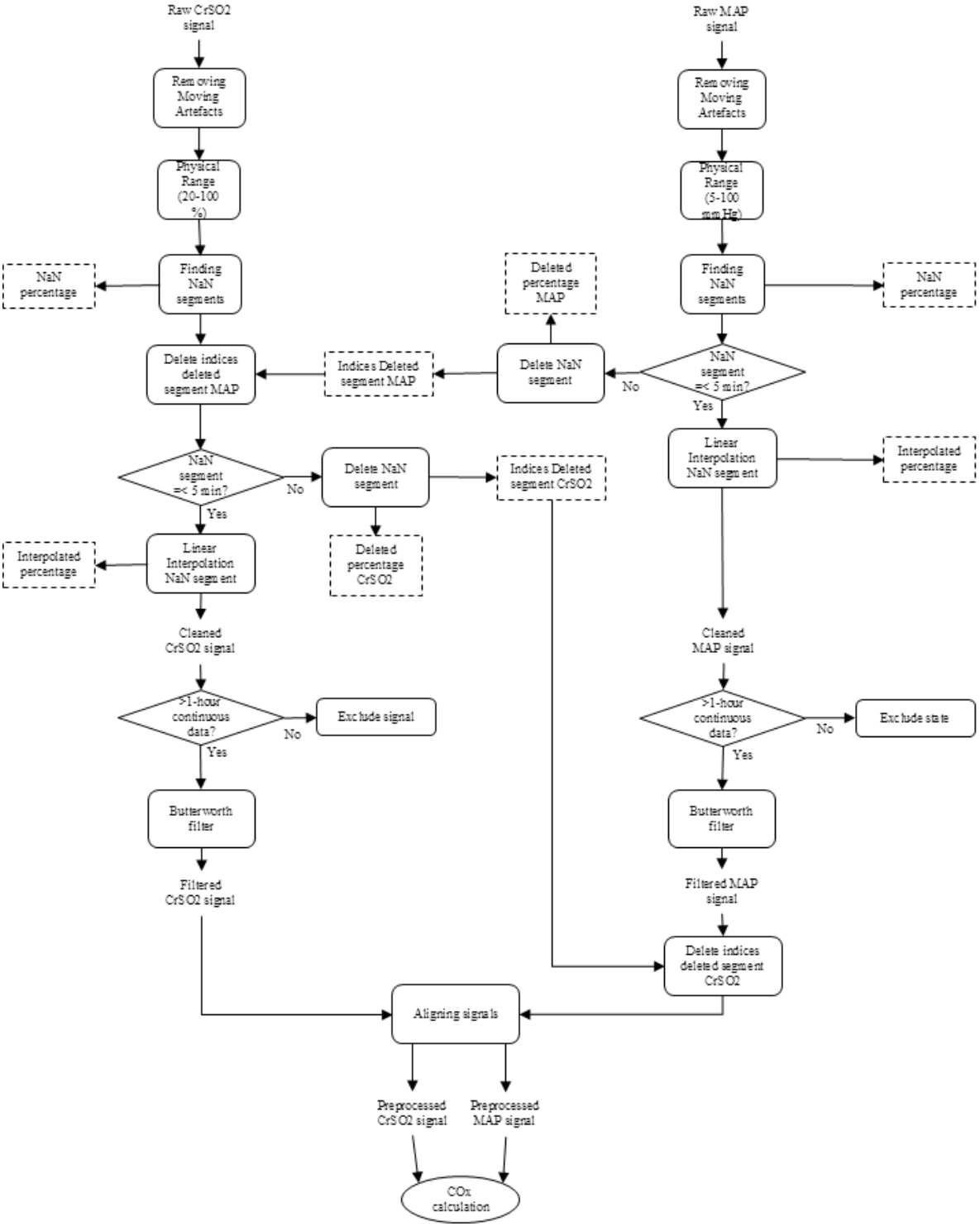

Figure A.1: Detailed schematic overview of the preprocessing pipeline.

A.3. Preprocessing Visualization: CrSO2

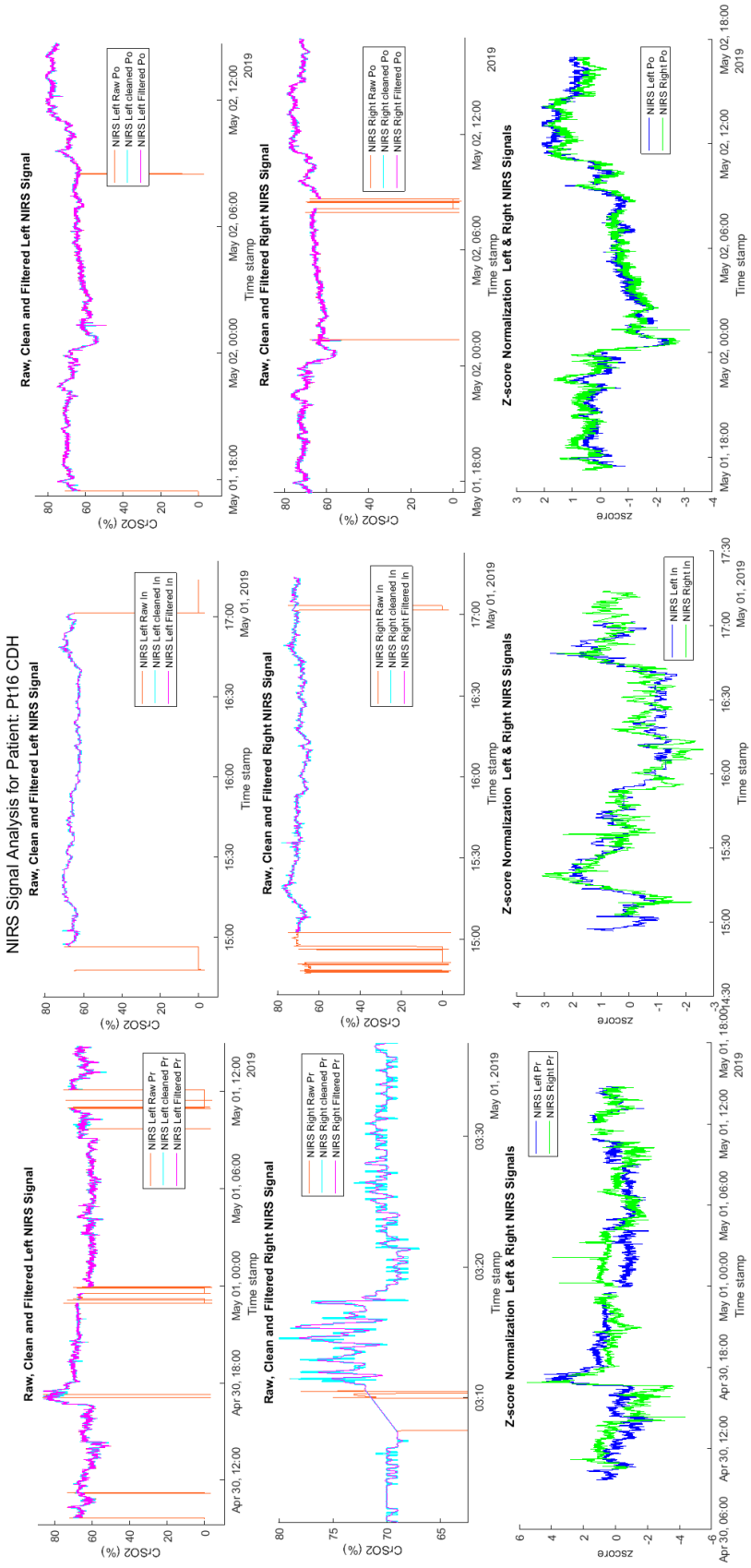

Figure A.2: Preprocessing of the CrSO2 signals of a random patient. The first column is the left CrSO2 signal, second row is the right CrsO2 signal and the third row is the normalization of the filtered left and right CrSO2 signals. The columns are divided into the operative windows. *Note:* The intraoperative right CrSO2 signal is zoomed in.

A.4. Scatterplots COx vs MAP_{opt}

CDH

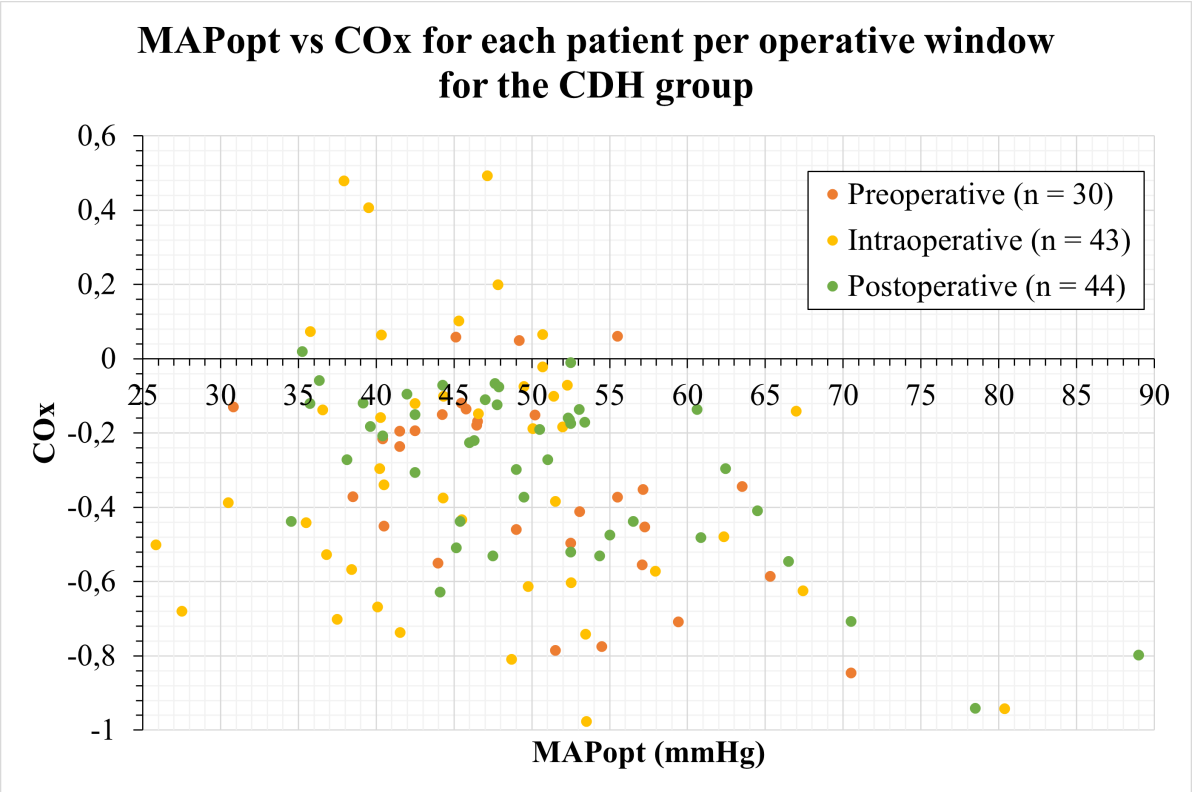

Figure A.3: Scatterplot of the MAP_{opt} values with their corresponding COx values per operative state for the CDH group.

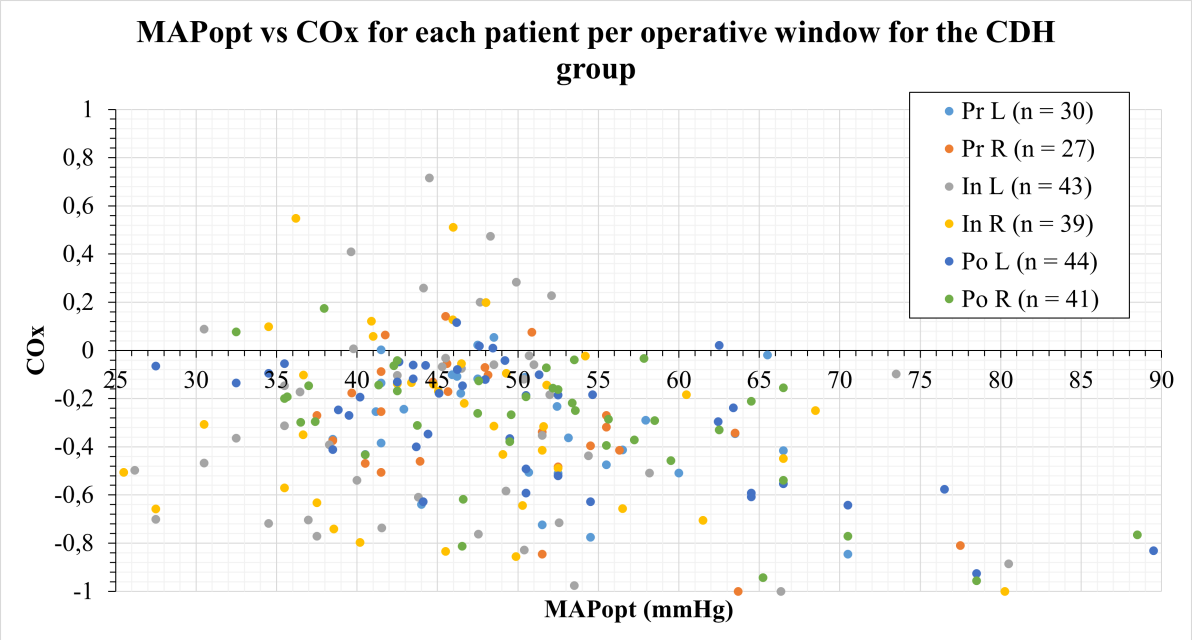

Figure A.4: Scatterplot of the MAP_{opt} values with their corresponding COx values per operative state per side for the CDH group.

EA

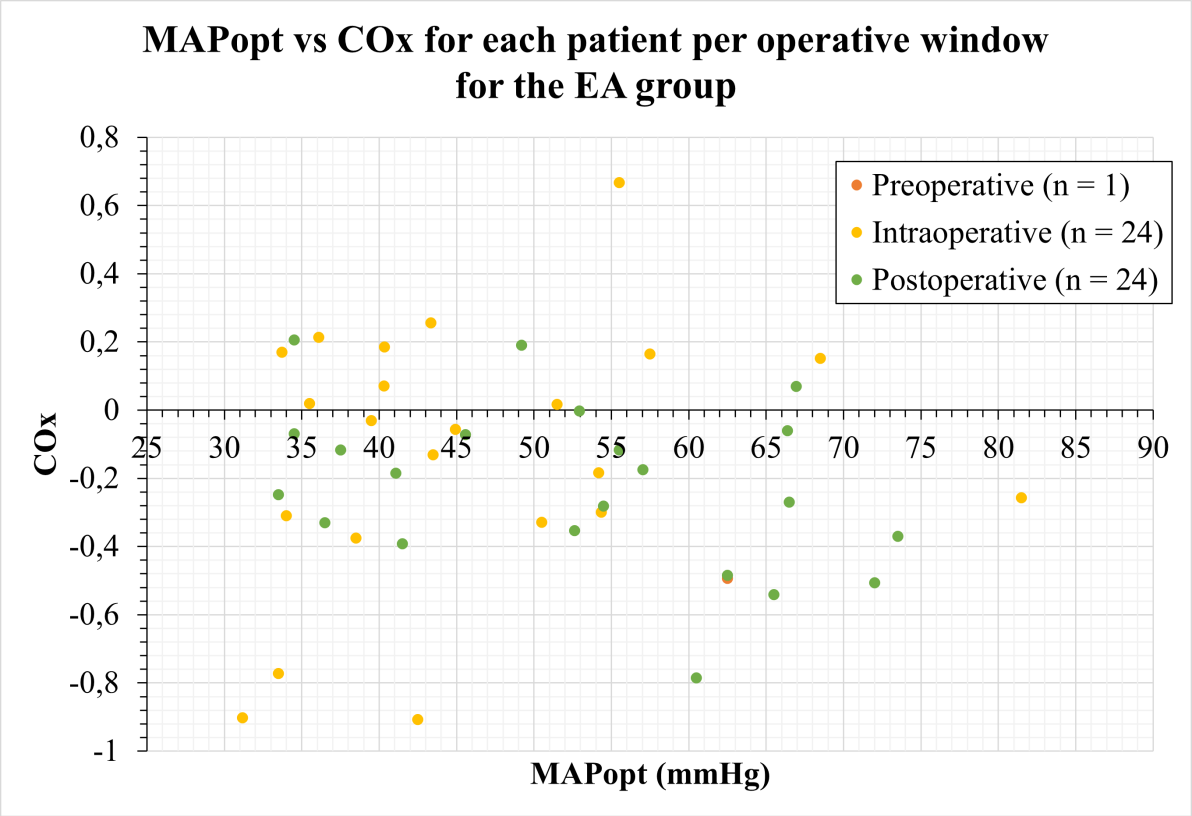

Figure A.5: Scatterplot of the MAP_{opt} values with their corresponding COx values per operative state for the EA group.

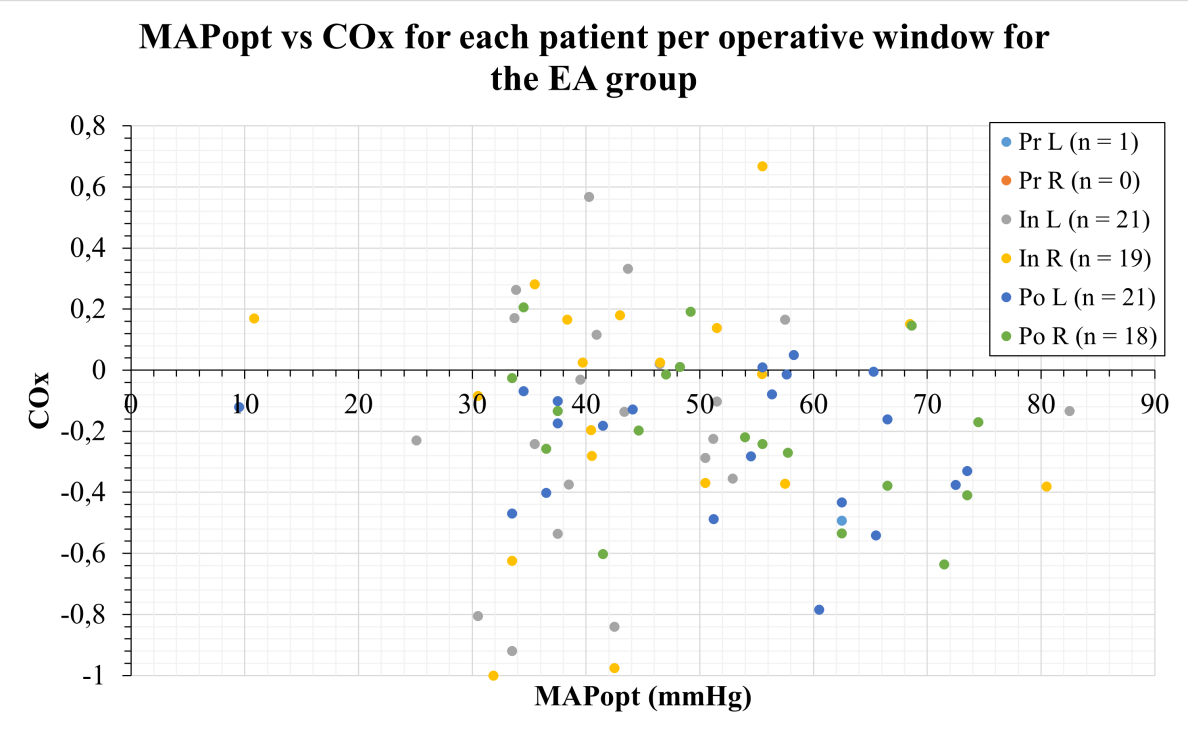

Figure A.6: Scatterplot of the MAP_{opt} values with their corresponding COx values per operative state per side for the EA group.

Per Operative Window

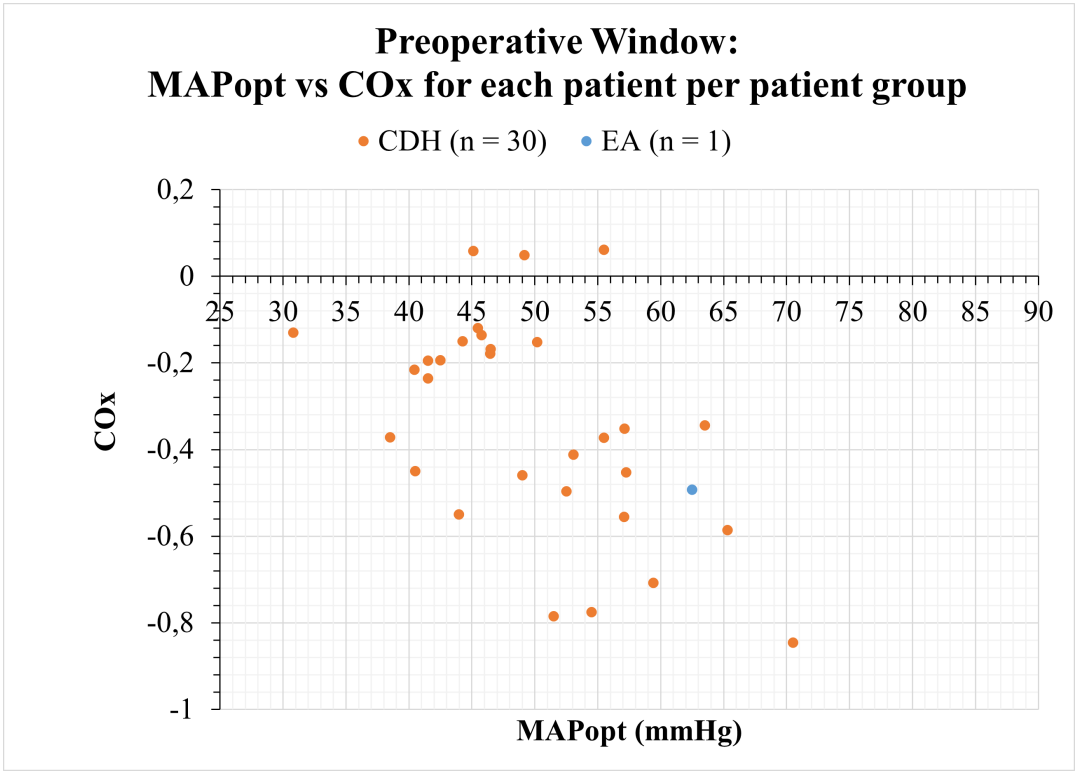

Figure A.7: Scatterplot of the MAP_{opt} values with their corresponding COx values per patientgroup for the preoperative window.

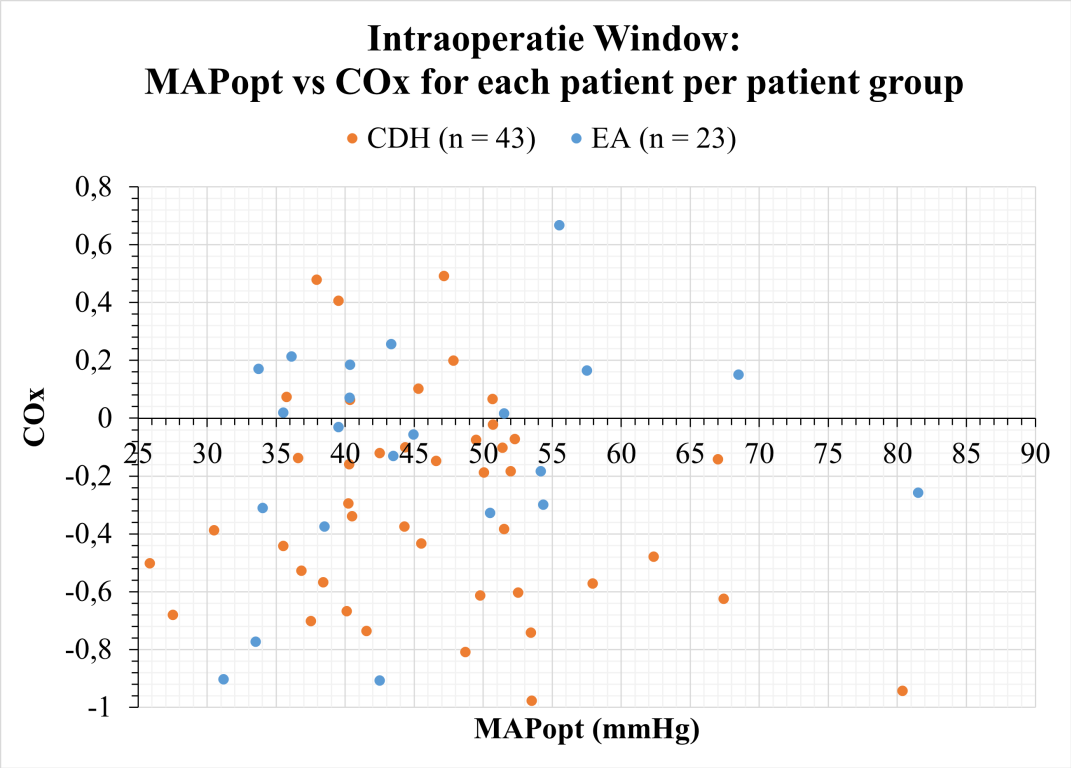

Figure A.8: Scatterplot of the MAP_{opt} values with their corresponding COx values per patientgroup for the intraoperative window.

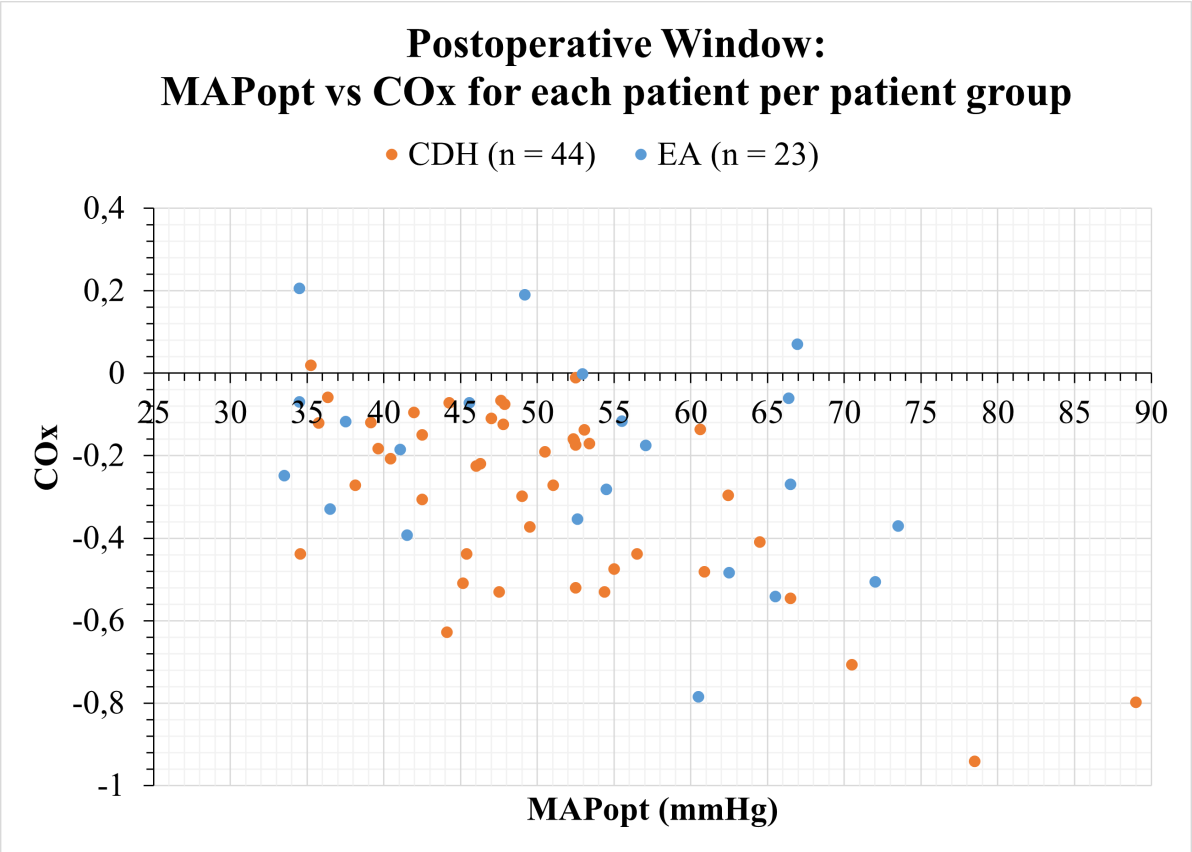

Figure A.9: Scatterplot of the MAP_{opt} values with their corresponding COx values per patientgroup for the Postoperative window.

A.5. Boxplots and Trends: Left and Right Seperate

COx

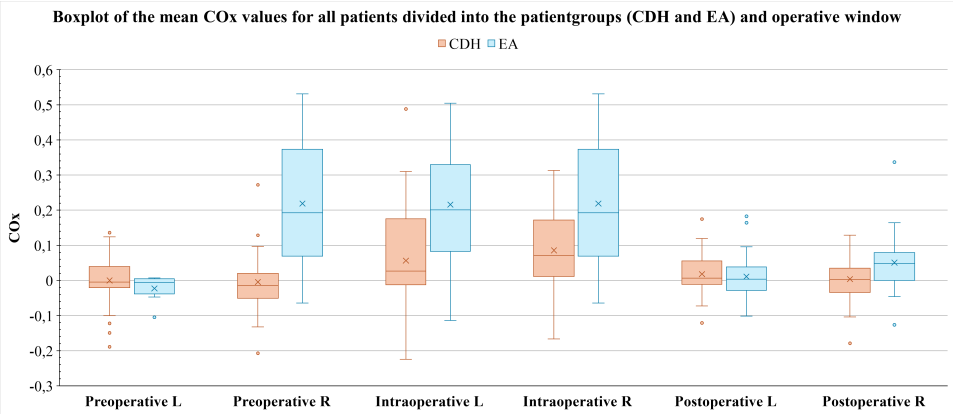

Figure A.10: Boxplot of the mean COx values combined to visualize the distribution of the mean COx values per side, operative window and patientgroup (CDH, EA).

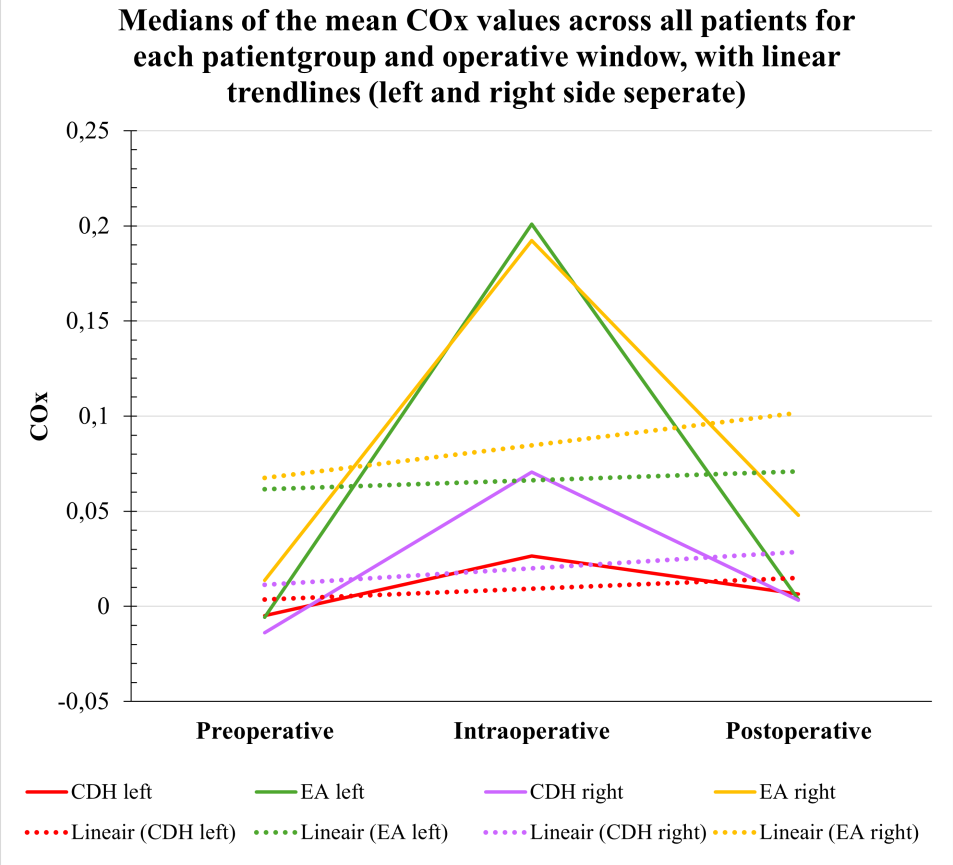

Figure A.11: Visualization of the trend of the median of the mean COx values per operative window and side for each patientgroup (CDH, EA) with a corresponding linear fit.

COx Above Cut-Off Value

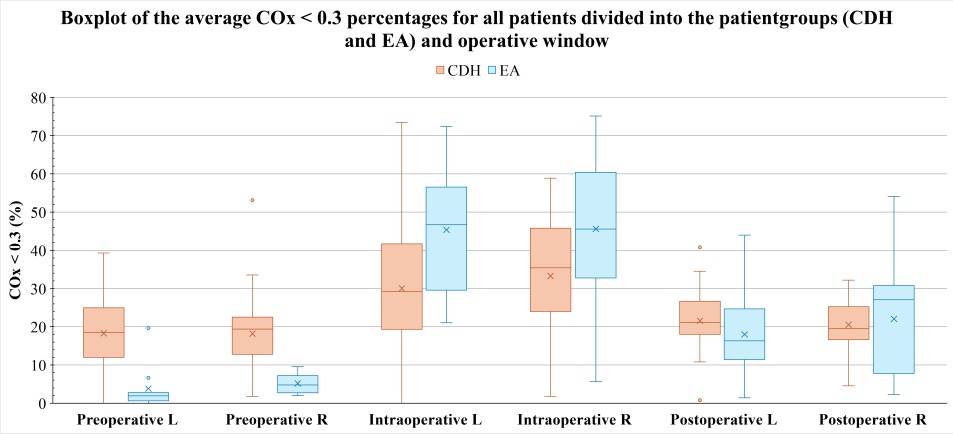

Figure A.12: Boxplot of the mean percentages of the total time for the operative window and side where the COx is above the cut off value to visualize the distribution per operative window and per patientgroup (CDH, EA).

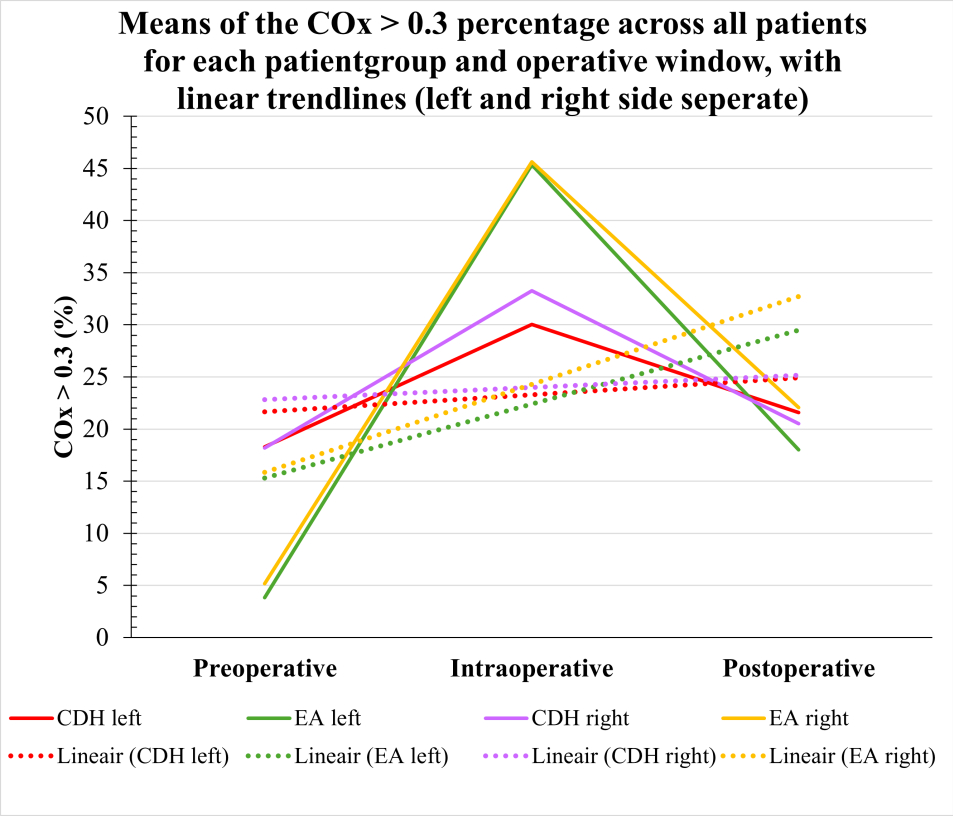

Figure A.13: Visualization of the trend of the mean of the mean percentages where the COx is above the cut off value per operative window and sidefor each patientgroup (CDH, EA) with a corresponding linear fit.

MAP_{opt}

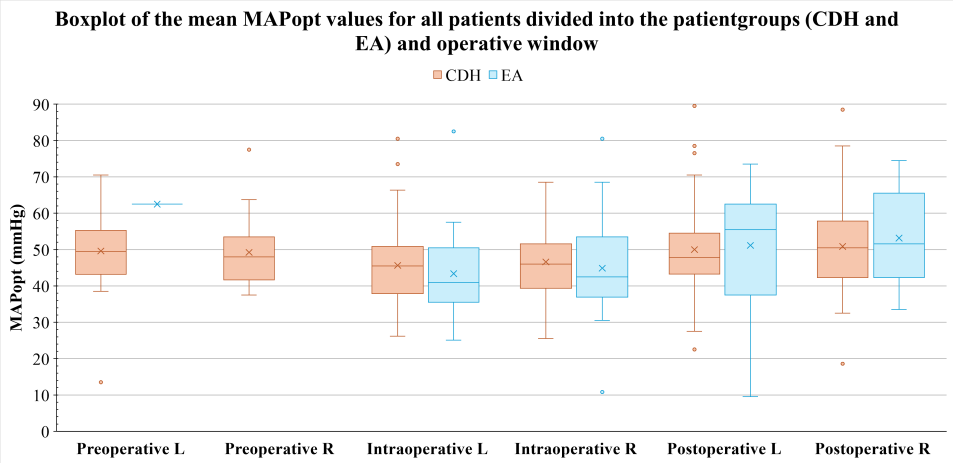

Figure A.14: Boxplot of the mean MAPopt values determined to visualize the distribution per operative window and side and per patientgroup (CDH, EA).

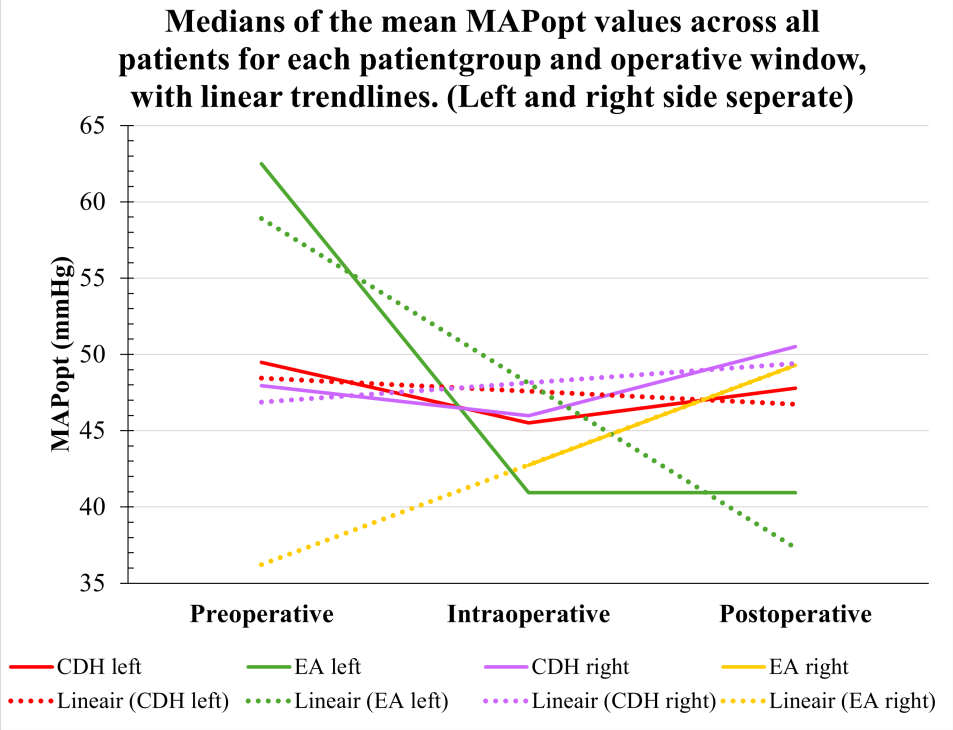

Figure A.15: Visualization of the trend of the medians of the mean MAPopt values per operative window and side for each patientgroup (CDH, EA) with a corresponding linear fit.

COx at MAP_{opt}

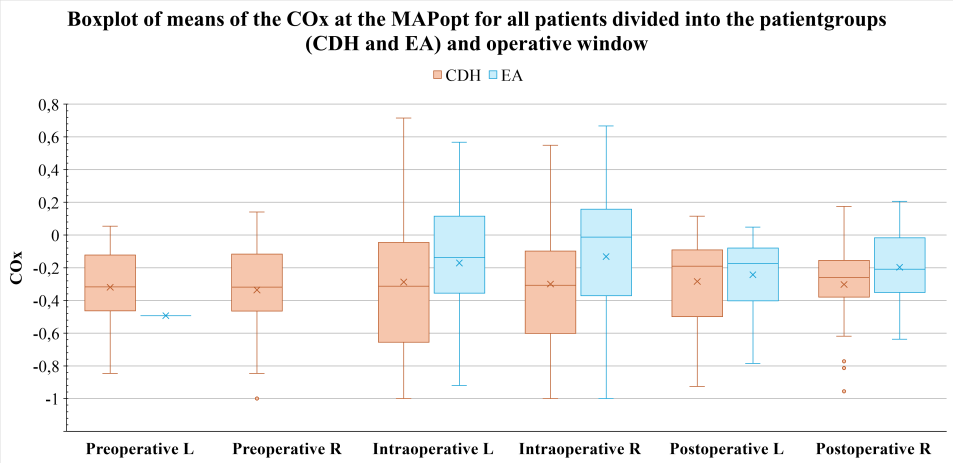

Figure A.16: Boxplot of the mean COx values at the MAPopt determined to visualize the distribution per operative window and side and per patientgroup (CDH, EA).

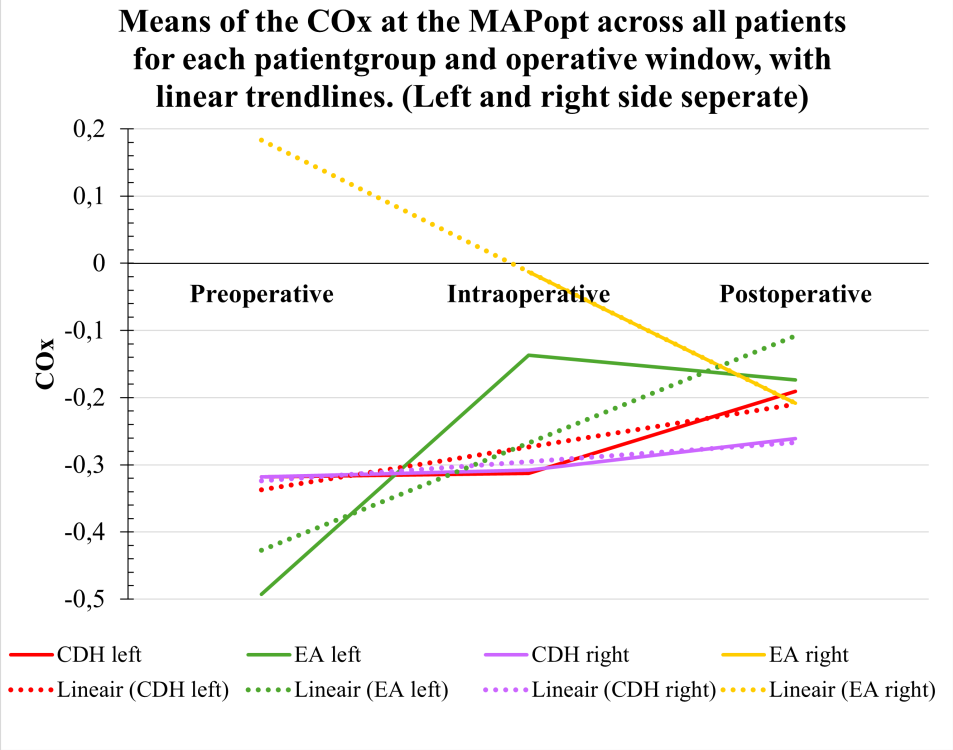

Figure A.17: Visualization of the trend of the medians of the mean COx values at the MAPopt per operative window and side for each patientgroup (CDH, EA) with a corresponding linear fit.